

Article

Pronounced Seasonal and Spatial Variability in Determinants of Phytoplankton Biomass Dynamics along a Near–Offshore Gradient in the Southern North Sea

Viviana Otero ^{1,†}, Steven Pint ^{1,*}, Klaas Deneudt ¹, Maarten De Rijcke ¹, Jonas Mortelmans ¹, Lennert Schepers ¹, Patricia Martin-Cabrera ¹, Koen Sabbe ², Wim Vyverman ², Michiel Vandegehuchte ¹ and Gert Everaert ¹

¹ Flanders Marine Institute, Jacobsenstraat 1, 8400 Ostend, Belgium; klaas.deneudt@vliz.be (K.D.); maarten.de.rijcke@vliz.be (M.D.R.); jonas.mortelmans@vliz.be (J.M.); lennert.schepers@vliz.be (L.S.); patricia.cabrera@vliz.be (P.M.-C.); gert.everaert@vliz.be (G.E.)

² Department of Biology, Ghent University, Krijgslaan 281-S8, 9000 Ghent, Belgium; koen.sabbe@ugent.be (K.S.); wim.vyverman@ugent.be (W.V.)

* Correspondence: steven.pint@vliz.be

† These authors contributed equally to this work.

Abstract: Marine phytoplankton biomass dynamics are affected by eutrophication, ocean warming, and ocean acidification. These changing abiotic conditions may impact phytoplankton biomass and its spatiotemporal dynamics. In this study, we used a nutrient–phytoplankton–zooplankton (NPZ) model to quantify the relative importance of the bottom-up and top-down determinants of phytoplankton biomass dynamics in the Belgian part of the North Sea (BPNS). Using four years (2014–2017) of monthly observations of nutrients, solar irradiance, sea surface temperature, chlorophyll-a, and zooplankton biomass at ten locations, we disentangled the monthly, seasonal, and yearly variation in phytoplankton biomass dynamics. To quantify how the relative importance of determinants changed along a near–offshore gradient, the analysis was performed for three spatial regions, i.e., the nearshore region (<10 km to the coastline), the midshore region (10–30 km), and the offshore region (>30 km). We found that, from year 2014 to 2017, the phytoplankton biomass dynamics ranged from 1.4 to 23.1 mg Chla m⁻³. Phytoplankton biomass dynamics follow a general seasonal cycle, as is the case in other temperate regional seas, with a distinct spring bloom (5.3–23.1 mg Chla m⁻³) and a modest autumn bloom (2.9–5.4 mg Chla m⁻³). This classic bimodal bloom pattern was not observed between 2003 and 2010 in the BPNS. The seasonal pattern was most expressed in the nearshore region. The relative contribution of factors determining phytoplankton biomass dynamics varied spatially and temporally. Throughout a calendar year, solar irradiance and zooplankton grazing were the most influential determinants in all regions, i.e., they jointly explained 38–65% of the variation in the offshore region, 45–71% in the midshore region, and 56–77% in the nearshore region. In the near- and midshore regions, nutrients were the greatest limit on phytoplankton production in the month following the spring bloom (44–55%). Nutrients were a determinant throughout the year in the offshore region (27–62%). During winter, sea surface temperature was a determinant in all regions (15–17%). By the high-resolution spatiotemporal analysis of the relative contributions of different determinants, this study contributes to a better mechanistic understanding of the spatiotemporal dynamics of phytoplankton biomass in the southern North Sea. This detailed understanding is anticipated to contribute to the definition of targeted management strategies for the BPNS and to support sustainable development in Belgium’s blue economy.

Keywords: primary production; ecosystem model; phytoplankton biomass dynamics; environmental conditions



Citation: Otero, V.; Pint, S.; Deneudt, K.; De Rijcke, M.; Mortelmans, J.; Schepers, L.; Martin-Cabrera, P.; Sabbe, K.; Vyverman, W.; Vandegehuchte, M.; et al. Pronounced Seasonal and Spatial Variability in Determinants of Phytoplankton Biomass Dynamics along a Near–Offshore Gradient in the Southern North Sea. *J. Mar. Sci. Eng.* **2023**, *11*, 1510. <https://doi.org/10.3390/jmse11081510>

Academic Editors: Vladimir Silkin and Sang Heon Lee

Received: 9 June 2023

Revised: 24 July 2023

Accepted: 26 July 2023

Published: 29 July 2023



Copyright: © 2023 by the authors. Licensee MDPI, Basel, Switzerland. This article is an open access article distributed under the terms and conditions of the Creative Commons Attribution (CC BY) license (<https://creativecommons.org/licenses/by/4.0/>).

1. Introduction

Marine phytoplankton, which forms the base of marine food webs, is responsible for about half of the world's total primary production [1]. Net global marine primary production is estimated at 50.7 Gt carbon per year [2]. Principal factors that determine marine primary production are solar irradiance, nutrient availability, and sea surface temperature (SST), and these factors mainly limit phytoplankton's growth rate and carrying capacity. According to Liebig's law of the minimum, phytoplankton production will be as high as allowed by the least available resource [3]. However, in many cases, co-limitation by resources is a better description of the factors that influence phytoplankton biomass dynamics [4,5]. Living in the Anthropocene, phytoplankton biomass dynamics are affected by human activities that directly or indirectly alter the abiotic marine environment, such as the burning of fossil fuels, eutrophication, and chemical pollution. To date, we have limited insight into how the combination of changing conditions may affect phytoplankton biomass dynamics at high-resolution spatiotemporal scales.

In temperate marine regions, phytoplankton biomass dynamics follow an annual cycle consisting of spring and autumn phytoplankton blooms, followed by periods of zooplankton grazing. Phytoplankton blooms are triggered by high nutrient availability and sufficient solar irradiance [6]. After a few weeks of rapid growth, phytoplankton biomass becomes restricted by nutrient limitation and zooplankton grazing. As in other parts of the North Sea, the most important factors that determine the phytoplankton biomass in the Belgian part of the North Sea (BPNS; 3454 km² [7]) are nutrient concentrations, SST, and solar irradiance [8–11]. Everaert et al. [12] is one of the first studies that quantified the relative importance of these conditions in the BPNS. Based on a relatively short time series at one location in the BPNS, it was found that SST and solar irradiance accounted for 20% (summer) to 50% (winter) of the observed seasonal variation [12] and can thus be considered potentially key determinants. Nutrients appeared to be less of a determinant than SST and solar irradiance in the BPNS [12], and this was also found to be the case for the entire North Sea by Llope et al. [13] and McQuatters-Gollop et al. [14]. Nutrients become the dominant determinant of phytoplankton biomass (30%) in the month after the phytoplankton bloom. Besides these bottom-up determinants, there is also a strong top-down control of phytoplankton biomass dynamics by zooplankton grazing, i.e., up to 50% of the phytoplankton growth limitation [12]. However, the BPNS is a heterogeneous and dynamic coastal area, so it is doubtful whether the quantifications in Everaert et al. [12] are generalisable for the entire BPNS. The BPNS is relatively shallow with water depths gradually increasing to 45 m from the southeast towards the northwest [15]. Sea surface temperatures vary seasonally between 5 °C and 20 °C. The salinity is strongly influenced by the river plumes of the Scheldt, Rhine, Seine, and Meuse [16], and it varies between 29 to 35 PSU. Seawater from the English Channel, which contains runoff from the Seine, flows northwards through the BPNS driven by the anti-clockwise current in the North Sea [17]. In the case of nutrients, the Seine plays a major role, except in the vicinity of the Scheldt estuary and in the northern part of the BPNS, i.e., it is mainly influenced by the influx of water from the Atlantic Ocean [18]. Due to its shallowness and riverine influx, there is a permanent vertical mixing of the water column in the BPNS [16]. Overall, in heterogeneous and dynamic coastal areas such as the BPNS, the relative contribution—i.e., how much a determinant contributes to the change in phytoplankton biomass in relation to the cumulative contribution of all determinants—of bottom-up and top-down determinants may be likewise dynamic, both spatially and temporally. The BPNS being a prime example of such a system in combination with the availability of long-term observations with high spatial resolution offers unique possibilities to study the scales at which the relative contributions of bottom-up and top-down determinants may shift. Having a better understanding of the spatial variation in the relative contribution of the determinants of phytoplankton biomass dynamics can lead to a more adjusted and specified management of the BPNS, as well as to the further development of the blue economy in Belgium.

In the present research, the aim is to analyse which factors drive marine phytoplankton biomass dynamics in the BPNS and how their relationship to primary production varies on a spatiotemporal scale. In particular, we analysed how the relative contributions of SST, nutrient regimes, solar irradiance, and zooplankton grazing to the marine phytoplankton biomass change, both spatially and temporally. We used a nutrient–phytoplankton–zooplankton (NPZ) model (obtained from Soetaert and Herman [19] and adjusted by Everaert et al. [12]) to simulate changes in plankton density in the nearshore, midshore, and offshore regions; this simulation was based on the monthly data collected from 2014 to 2017 at ten sampling locations in the BPNS. The novelty of this study lies in its high-resolution spatiotemporal analysis, which examines the varying impacts of potential determinants on phytoplankton biomass. The high spatiotemporal analysis contributes to a better understanding of phytoplankton biomass dynamics in the BPNS. It is anticipated that this comprehensive exploration has the potential to guide more focused management strategies for the BPNS and could bolster sustainable development within Belgium’s blue economy.

2. Materials and Methods

2.1. Input Data

Three regions of interest were studied (Figure 1), i.e., the nearshore region (10 km), the midshore region (10–30 km), and the offshore region (>30 km). These regions were defined based on an integration of information about their distance to the coast, their sediment composition, bathymetry [20,21], and prior knowledge about different abiotic conditions [22]. LifeWatch measuring stations are located in each of these regions (indicated as triangles in Figure 1). LifeWatch is a European research infrastructure within the European Strategy Forum on Research (ESFRI) that focuses on biodiversity research and activities, such as measuring the biotic and abiotic environment. LifeWatch stations in the near- and midshore are visited monthly [23]. We used data from two stations, i.e., 130 for nearshore and 330 for midshore, as well as pooled the data of seven sampling stations for the offshore region (Figure 1). The data of all offshore stations, i.e., seven stations, were pooled in this study due to the lower temporal sampling. In the offshore region, the LifeWatch stations are visited seasonally, whereas stations in the near- and midshore are visited monthly.

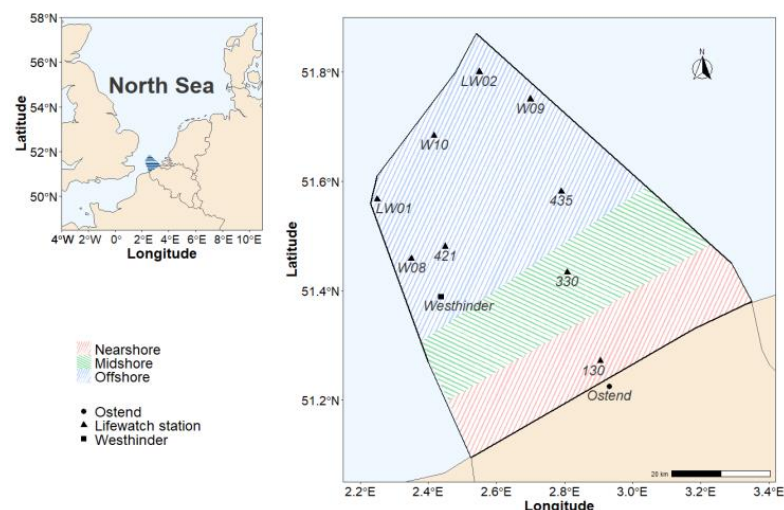


Figure 1. Map of the Belgian part of the North Sea (BPNS) showing the sampling locations used in this study for the near-, mid-, and offshore regions. The square mark shows the Westhinder station from the Flemish Banks Monitoring Network in the BPNS. The black outline indicates the Belgian Exclusive Economic Zone.

Four open-access datasets obtained from LifeWatch sampling campaigns, which are coordinated by the Flanders Marine Institute, at nine locations in the BPNS from 2014 to

2017 were used [23–26]. A first open-access dataset related to the nutrient concentrations, i.e., NH_4 , NO_3 , NO_2 , PO_4 , and SiO_3 , was used and the measurements were performed by a Skalar AutoAnalyser system [23,25]. A second open-access dataset consisted of seawater temperature measurements, and this was performed by a CTD [25]. Environmental measurements were taken at a depth of three metres. A third open-access dataset comprised zooplankton abundances, which were obtained through ZooScan analysis [24,26]. A fourth and final dataset used in this research contained information on the in situ pigment concentrations, i.e., chlorophyll-a, and these measurements were performed by HPLC [23,25]. The pigment concentrations were the result of pigment purification and sample analysis, i.e., obtained by taking the cumulative sum of phytoplankton taxa found in the water column. By doing so, the model takes into account the presence of phytoplankton taxa in the BPNS.

The gathered data were assembled in two new datasets: the first containing the data related to nutrient and pigment concentrations, as well as seawater temperature; the second containing the zooplankton abundances. The zooplankton dataset contains the abundances of the following taxa, as they are the most abundant in the BPNS (Appendix C [27]): Calanoida, Noctiluca, Harpacticoida, and Appendicularia. All data were timestamped and were location-specific.

In addition to the SST dataset gathered from LifeWatch, a second SST dataset with a higher temporal coverage was required to infer the daily time series, i.e., the input data for our nutrient–phytoplankton–zooplankton model, which was achieved by means of generalised additive models. The SST data from the Westhinder station, i.e., the data from the Westhinder measuring pile, was complemented with data from the Westhinder–buoy (2% of the dataset). This station is part of the Flemish Banks Monitoring Network [28], and their SST data was used to infer the daily time series for nutrients and the SST. Due to large data gaps in the SST dataset of the Westhinder station in 2018, we have chosen to use the dataset from 2014–2017 in order to avoid increasing random noise when calibrating the model by including an extra dataset of the SST.

2.2. Time Trends for Input Data

Generalised additive models (GAM) were used to infer the daily trends for nutrient concentrations, i.e., N, P, and Si, in the three regions of interest (Appendix C). These daily trends were based on the monthly and seasonal data collected via LifeWatch. The daily time series were used as input for the nutrient–phytoplankton–zooplankton model. Dissolved inorganic nitrogen (DIN) was calculated as the sum of ammonium (NH_4^+), nitrate (NO_3^-), and nitrite (NO_2^-). Measurements of NH_4 , NO_3 , NO_2 , PO_4 , and SiO_3 registered in the LifeWatch database were already converted into nitrogen, phosphorus, and silica equivalent weights, respectively. The covariates used in the GAM models were month and year, as in Everaert et al. [12], to infer the daily trends. The model fit of the GAMs was assessed following the method of Zuur et al. [29], i.e., using the Akaike Information Criterion (AIC) and inspecting the homogeneity and normality of the model residuals. The AIC was calculated via the package ‘stats’ [30], and the minimum AIC was used to select the best-fit GAM models (Table A7). The corresponding R^2 of the best-fit GAM model provides an indication of how well the model fits the observational data (Table A6).

The daily SST for the near- and midshore stations were calculated using GAM models that were based on the temperature observations from LifeWatch. For the offshore region, the SST data of the Westhinder station (Figure 1) were used. In the case that multiple temperature loggings were available per day, the median daily SST was used as the input for the model.

2.3. Ecological Model

A nutrient–phytoplankton–zooplankton (NPZ) model as presented in Everaert et al. [12] (Figure 2), which was adjusted from Soetaert and Herman [19], was used to simulate spatiotemporal changes in plankton density in the BPNS from 2014 to 2017. The model

time step is expressed in $\text{mmol N m}^{-3} \text{d}^{-1}$, and the state variables are expressed in mmol N m^{-3} . The necessary input data for the NPZ model are (i) nutrient concentrations, (ii) SST, and (iii) solar irradiance (Photosynthetically Active Radiation (PAR)), which is corrected for the diffusion attenuation coefficient (the K_d is calculated at a three-metre depth; Equation (10)). The PAR and nutrients, i.e., DIN, PO_4 , and SiO_3 , were implemented in the NPZ model as saturating Michaelis–Menten equations, as shown in Arndt et al. [8]. As such, the Michaelis–Menten equations describe the determining factor of a variable of interest, i.e., PAR, DIN, PO_4 , or SiO_3 , for each time step. The outcome of these equations varies from one to zero, with a value of one indicating no limitation for plankton growth, and a value of zero indicating a complete limitation of the plankton growth [19]. Both the vertical and horizontal mixing of nutrients were incorporated in the model as they were inherently included in the in situ observations used to calibrate and fit our model. The amount of PAR available was corrected for the diffuse attenuation coefficient by means of the Lambert–Beer law [31,32]. The same fixed sinusoidal surface irradiance for all three regions was used as the angle of the sunlight and surface, and light hours were assumed to be the same across all regions in our small study area. The influence of the SST on plankton growth followed the Thomann and Mueller [33] equation (Equation (6)) [12]. The NPZ model and corresponding calculations were performed in R [30] (version 3.4.4; R packages ‘doParallel’ [34], ‘dplyr’ [35], ‘foreach’ [36], ‘ggplot2’ [37], ‘ggpubr’ [38], ‘lubridate’ [39], ‘parallel’ [30], ‘plyr’ [40], ‘RColorBrewer’ [41], ‘reshape2’ [42], ‘stats’ [30], ‘viridis’ [43], and ‘xts’ [44]).

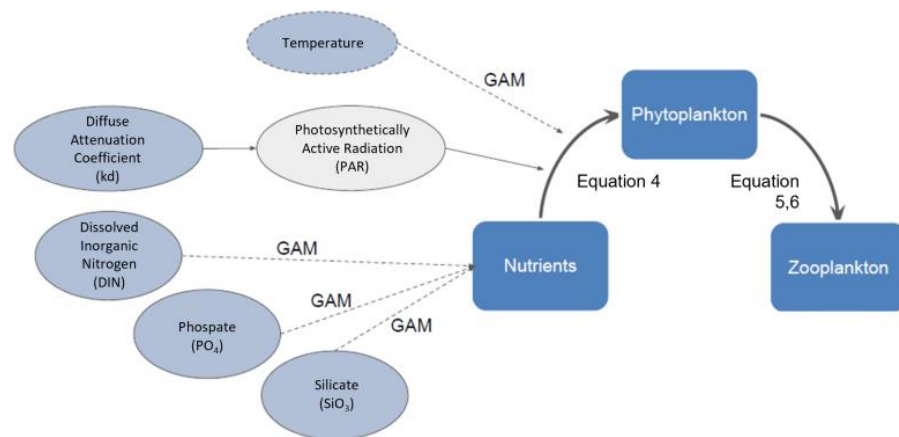


Figure 2. Structure of the nutrient–phytoplankton–zooplankton ecological model. Input data such as dissolved inorganic nitrogen (DIN), phosphate (PO_4), and silicate (SiO_3) concentration, as well as the photosynthetically active radiation, were obtained from LifeWatch. The sea surface temperature was obtained from LifeWatch and the Flemish Banks Monitoring Network. The generalised additive models (GAMs) were used to obtain daily data for nutrients based on monthly observations (see Section 2.1).

The equation-based description of the model is presented following the state variables of the model (set according to Soetaert and Herman [19]). Nutrients were depicted as regression-based models, i.e., for nitrogen GAM_{DIN} , phosphorus GAM_{PO_4} , and silica $\text{GAM}_{\text{SiO}_3}$ (Equation (1)).

$$\text{Nutrients} = \text{GAM}_{\text{DIN}} + \text{GAM}_{\text{PO}_4} + \text{GAM}_{\text{SiO}_3} \tag{1}$$

The differential equations determined the rates of change in the biomass of phytoplankton ($d\text{PHYTO}$; Equation (2)) and zooplankton ($d\text{ZOO}$; Equation (3)).

$$\frac{d\text{PHYTO}}{dt} = N_{\text{uptake}} - \text{Grazing} \tag{2}$$

$$\frac{dZOO}{dt} = \text{Grazing} - \text{Faeces} - \text{Excretion} - \text{Mortality} \tag{3}$$

where t indicates time in days; N_{uptake} , the phytoplankton’s nutrient uptake; Grazing, the rate of grazing of zooplankton on phytoplankton; Faeces, the faeces production of zooplankton; Excretion, the zooplankton excretion; and Mortality, the mortality of zooplankton. N_{uptake} is the phytoplankton’s nutrient uptake, which was expressed as the maximum uptake of nutrients (maxUptake) and is limited by the following: solar irradiation (Par_{lim}), SST (Temp_{lim}), the concentrations of nitrogen (DIN_{lim}), phosphorus (P_{lim}), and silica (Si_{lim}) expressed as limitation factors, and the phytoplankton biomass (PHYTO; Equation (4)). The equations used to define the limitation factors follow the saturating Michaelis–Menten equations [19]:

$$N_{\text{uptake}} = \text{maxUptake} \cdot \text{Par}_{\text{lim}} \cdot \text{Temp}_{\text{lim}} \cdot \text{P}_{\text{lim}} \cdot \text{DIN}_{\text{lim}} \cdot \text{Si}_{\text{lim}} \cdot \text{PHYTO} \tag{4}$$

$$\text{Par}_{\text{lim}} = \frac{\text{PAR}}{\text{PAR} + k_{\text{SPAR}}} \tag{5}$$

$$\text{Temp}_{\text{lim}} = \theta^{\text{Temp} - T_{\text{obs}}} \tag{6}$$

$$\text{DIN}_{\text{lim}} = \frac{\text{DIN}}{\text{DIN} + k_{\text{SDIN}}} \tag{7}$$

$$\text{P}_{\text{lim}} = \frac{\text{P}}{\text{P} + k_{\text{SP}}} \tag{8}$$

$$\text{Si}_{\text{lim}} = \frac{\text{Si}}{\text{Si} + k_{\text{SSi}}} \tag{9}$$

where k_{SPAR} , T_{obs} , k_{SDIN} , k_{SP} , and k_{SSi} are parameters of the model. The equation for PAR (Equation (10)) is defined based on the Lambert-Beer law [31,32]. where I_0 is the surface irradiance ($\mu\text{Einst m}^{-2} \text{s}^{-1}$), z is the depth (m), and k_d is the diffuse attenuation coefficient (m^{-1}).

$$\text{PAR} = I_0 \cdot e^{-k_d \cdot z} \tag{10}$$

$$\theta = 1.185 - 0.00729 \cdot \text{Temp} \tag{11}$$

In the model, the surface irradiance is modelled as photosynthetically active radiation, as defined in Soetaert and Herman [19]:

$$I_0 = 0.5 \cdot \left(540 + 440 \cdot \sin\left(\frac{2 \cdot \pi \cdot t}{365 - 1.4}\right) \right) \tag{12}$$

where t indicates the day of the year. The diffuse attenuation coefficient (k_d) describes the rate at which light diminishes with depth due to absorption and scattering in the water column [31,32,45]. K_d is used as a proxy of the influence of Suspended Particulate Matter (SPM) on the PAR [45]. The K_d values were calculated based on the PAR and depth data recorded in the Marine Information and Data Acquisition System (MIDAS). The depth (z) used in Equation (10) was at three metres as the LifeWatch data are measured at a three-metre depth [23].

Grazing represents the grazing of zooplankton (ZOO) on phytoplankton (PHYTO), i.e., how much biomass is eaten, and it is expressed as follows:

$$\text{Grazing} = \text{max}_{\text{Grazing}} \cdot \frac{\text{PHYTO}}{\text{PHYTO} + k_{\text{SGrazing}}} \cdot \text{ZOO} \tag{13}$$

where $\text{max}_{\text{grazing}}$ is the maximum phytoplankton biomass that can be eaten by zooplankton, and k_{sgrazing} is the half-saturation constant for grazing.

Zooplankton faeces production (Faeces) is expressed as a constant fraction (pFaeces) of the total grazing.

$$\text{Faeces} = \text{pFaeces} \cdot \text{Grazing} \tag{14}$$

Zooplankton excretion (Excretion) is estimated as the excretion rate (excretionRate) multiplied by the zooplankton biomass.

$$\text{Excretion} = \text{excretionRate} \cdot \text{ZOO} \tag{15}$$

Zooplankton mortality is determined by multiplying the mortality rate (mortalityRate) with the zooplankton biomass squared.

$$\text{Mortality} = \text{mortalityRate} \cdot \text{ZOO}^2 \tag{16}$$

The phytoplankton biomass is converted to a chlorophyll-a concentration by multiplying the phytoplankton biomass with the chlorophyll-a-to-nitrogen ratio.

$$\text{Chlorophyll} = \text{chlNratio} \cdot \text{PHYTO} \tag{17}$$

The maxUptake, excretionRate, maxGrazing, ks_{Grazing}, pFaeces, mortalityRate, and chlNratio are parameters of the model of which the seasonal ranges are provided for each region (Table 1).

Table 1. The seasonal minimum and maximum values of the thirteen parameters used as the input for the nutrient-phytoplankton-zooplankton model for each region.

Parameter	Unit	Period	Nearshore Region	Midshore Region	Offshore Region
maxUptake	day ⁻¹	Spring	0.38–0.66	0.38–0.61	0.50–1.12
		Autumn	0.40–0.78	0.38–0.80	0.38–0.90
excretionRate	day ⁻¹	Spring	0.16–0.18	0.12–0.16	0.11–0.15
		Autumn	0.11–0.17	0.11–0.15	0.11–0.14
maxGrazing	day ⁻¹	Spring	0.87–0.96	0.85–0.92	0.88–0.97
		Autumn	0.88–0.96	0.85–0.93	0.89–0.97
ks _{Grazing}	mmol N m ⁻³	Spring	2.15–3.27	1.54–2.15	1.48–2.22
		Autumn	1.31–2.27	1.19–1.59	1.25–1.94
pFaeces	day ⁻¹	Spring	0.29–0.41	0.27–0.40	0.27–0.40
		Autumn	0.25–0.40	0.24–0.32	0.25–0.37
mortalityRate	(mmol N m ⁻³) ⁻¹ day ⁻¹	Spring	0.28–0.39	0.28–0.41	0.29–0.41
		Autumn	0.32–0.44	0.35–0.42	0.33–0.45
ChlNratio	mg Chla (mmol N) ⁻¹	Spring	7.00–7.86	6.78–7.60	6.65–7.47
		Autumn	6.62–7.55	5.33–6.84	4.33–6.61
k _{SPAR}	μEinst m ⁻² s ⁻¹	Spring	126–227	133–224	103–210
		Autumn	121–205	126–200	115–210
T _{obs}	°C	Spring	9.86–13.84	10.11–13.29	9.54–13.62
		Autumn	10.41–12.83	9.66–13.86	10.08–13.62
ks _{DIN}	mmol N m ⁻³	Spring	1.33–4.21	1.62–3.94	1.92–3.70
		Autumn	1.17–3.64	2.22–4.11	2.07–4.29
k _{SP}	mmol P m ⁻³	Spring	0.30–0.43	0.28–0.44	0.30–0.44
		Autumn	0.33–0.40	0.29–0.46	0.30–0.44
ks _{Si}	mmol Si m ⁻³	Spring	0.41–0.66	0.43–0.67	0.34–0.67
		Autumn	0.35–0.63	0.40–0.67	0.39–0.65
K _d *	m ⁻¹	Spring	0.73–0.90	0.44–0.60	0.28–0.38
		Autumn	0.77–0.92	0.45–0.60	0.28–0.38

* Calculated at a three-metre depth.

2.4. Selection of Model Parameters and Validation

The NPZ model requires parameterisation of thirteen parameters (Tables 1 and A4). For the model parameterisation, we followed a two-step approach to find the most optimal model calibration for each region of the BPNS to mimic the biogeochemical processes in

each respective region (Figure 3). In a first step, 5000 unique sets of parameters, which were selected using a Monte Carlo approach, were run for each region of interest. The initial minimum and maximum parameter values used to define these unique sets of parameters were based on values reported in the literature (Table A1). In a second step, a new set of 5000 unique parameterisations, which were selected using a Monte Carlo approach, were run for each region of interest and for two seasons, i.e., spring and autumn. In this second step, the minimum and maximum parameter values were based on the 10% best parameterisation for either spring or autumn conditions from the first step. To rank these 10% best models, we calculated the Root Mean Square Error (RMSE) by comparing the NPZ model predictions of phyto- and zooplankton density with the observed pigment chlorophyll-a [25], i.e., a proxy for phytoplankton biomass and zooplankton densities [26], respectively. We calculated the total RMSE for each unique parameterisation as the cumulated error for phytoplankton and zooplankton. For each unique model parameterisation that we tested, we cumulated the error over the different time steps. We considered the best parameterisations as those with the lowest 10% RMSE. In this second step, we retained a set of parameters (Table 1) to describe the spring conditions, i.e., the situation after winter solstice and before summer solstice, and a set of parameters to describe the autumn conditions, i.e., the situation after summer solstice and before winter solstice. The two parameter sets were used to describe the changes in the environmental conditions in each season.

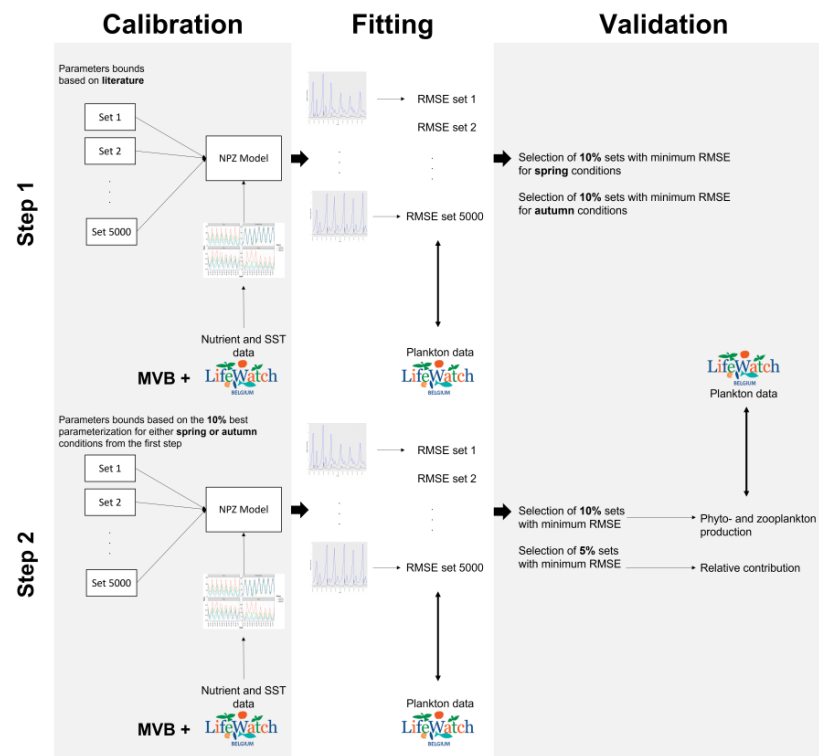


Figure 3. The key steps of model development, i.e., calibration, fitting, and validation. In a first step, 5000 unique sets of parameters were run for each region of interest. The initial minimum and maximum parameter values used to define these unique sets of parameters were based on values reported in the literature (Appendix A). The nutrient–phytoplankton–zooplankton (NPZ) model is driven by daily nutrient and sea surface temperature data generated from LifeWatch and Flemish Banks Monitoring Network observations. In a second step, a new set of 5000 unique parameterisations were run for each region of interest and for two seasons, i.e., spring and autumn. In this second step, the minimum and maximum parameter values were based on the 10% best parameterisation for either spring or autumn conditions from the first step. To rank these 10% best models, we calculated the Root Mean Square Error (RMSE) by comparing the NPZ model predictions of phyto- and zooplankton density with the observed pigment chlorophyll-a and zooplankton densities, respectively.

To assess the model fit, we compared the NPZ phytoplankton biomass predictions (expressed in mmol N m^{-3}) with the observed phytoplankton biomass data (expressed in mg Chla m^{-3}). To enable the comparison, we converted the unit of the NPZ phytoplankton biomass predictions and the unit of the LifeWatch phytoplankton biomass data to mg Chla m^{-3} . To do so, we used the Chl:N ratio parameter of the corresponding simulation (Table 1). To compare the NPZ zooplankton production predictions (expressed in mmol N m^{-3}) with the LifeWatch zooplankton observations (expressed in ind m^{-3}), we converted the latter to the same unit. To do so, we calculated the taxon-specific body mass per individual (mg C ind^{-1}), converted this mass to a molar mass (mmol C m^{-3}), and used a taxon-specific C:N ratio to finally convert the molar mass to mmol N m^{-3} . Details about this conversion are available in Appendix C (Tables A4 and A5). In addition, the model predictions were visually inspected by plotting the observed values against the predicted values (Figures A5 and A6). The visual inspection was used to evaluate the seasonality aspect of the model fit and to what extent that the models that obtained a good RMSE also corresponded to the ecological interactions and dynamics in one growth season. This visual inspection was performed to unravel the over- or underestimation of the model.

2.5. Relative Contributions

The relative importance of the SST, PAR, DIN, PO_4 , SiO_3 , and zooplankton grazing for phytoplankton biomass dynamics were calculated as was performed in Everaert et al. [12]. To do so, we made use of the forcing functions that were integrated in the model (cfr. 2.3). For each determinant, the absolute limitation was calculated as one minus the limitation factor. Then, the relative contribution of each determinant was calculated as the absolute limitation divided by the sum of all absolute limitations. Afterwards, the monthly relative contribution of each determinant was calculated based on the average relative contribution of the 5% best simulations, i.e., the simulations with the lowest RMSE, for each region of interest. The 5% best simulations were selected for calculating the monthly relative contribution as they offered a good compromise between computational cost and performance. The normality and homogeneity of the relative contribution data were tested, using the packages 'stats' [30] and 'lawstat' [46], by means of the Shapiro–Wilk test ($p < 0.05$) and the Levene's test ($p < 0.05$), respectively. Potential differences in the determinants between regions were examined using the Kruskal–Wallis test ('stats' package; [30]) and the Dunn test ('dunn.test' package; [47]) in R [30].

3. Results

3.1. Model Fit

The GAMs were used to create a daily time series of the nutrients and the SST, and were based on the monthly and seasonal observed data (Figure A4). The SST had the highest R^2 values, and the parameter with the lowest R^2 varied between regions (Table A6).

To assess the model fit, the model predictions of the phyto- and zooplankton were compared to the field observations, i.e., the RMSE was calculated for each unique parameterisation. The nearshore region had a total RMSE of 1.24–1.38. The mid- and offshore regions had a total RMSE of 0.39–0.46 and 0.32–0.42, respectively. We found that the RMSE for the phytoplankton in the nearshore region was 1.09–1.31, midshore was 0.30–0.40, and offshore was 0.26–0.38. The model tended to overestimate the phytoplankton density at low observed densities (Figure A5). At high observed phytoplankton densities, the model performs better (Figure A5). For the zooplankton, the RMSE was 0.07–0.23 in the nearshore, 0.06–0.13 in the midshore, and 0.04–0.09 in the offshore region. A similar pattern was observed for the zooplankton densities (Figure A6). In the offshore region, it was observed that the underestimation at high zooplankton densities was more pronounced (Figure A6).

3.2. Phytoplankton Time Trends

We found clear spatial differences in the phytoplankton biomass dynamics in the BPNS. The closer to the coastline, the higher the amplitude of the spring phytoplankton bloom and the more distinct the seasonal pattern (Figure 4). In the nearshore region, the phytoplankton biomass ranged from 3.5 to 23.1 mg Chla m^{-3} and followed a clear seasonal trend, with the highest chlorophyll-a concentration being observed in spring and the lowest chlorophyll-a concentration found in the winter (Figure 4). In the midshore region, the maximum phytoplankton biomass was estimated to be 8.8 mg Chla m^{-3} , and the minimum phytoplankton biomass was 1.8 mg Chla m^{-3} (Figure 4). In the offshore region, the spring blooming periods were still noticeable but less prominent (1.4–5.3 mg Chla m^{-3}) in terms of absolute phytoplankton biomass when compared to the nearshore region. In each of the selected regions, the autumn blooming periods were noticeable, but they became relatively more pronounced with an increasing distance from the coastline (Figure 4). Overall, the spring blooms were observed for each region and were followed by a smaller peak at the end of summer (Figure 4).

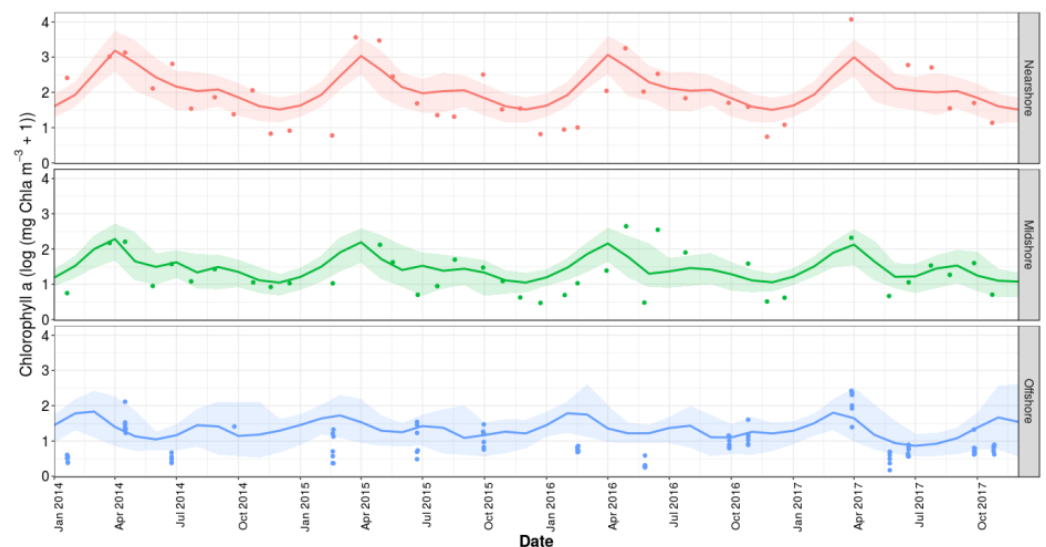


Figure 4. Phytoplankton biomass simulations using the nutrient–phytoplankton–zooplankton model in the nearshore, midshore, and offshore regions in the Belgian part of the North Sea. The bold lines indicate the average phytoplankton biomass predictions, and the shaded areas indicate the 95% confidence interval. The dots are the observed values collected during the LifeWatch campaigns.

We observed a response in the zooplankton population to the spring phytoplankton bloom (Figures 5 and A10). As theoretically expected from a classic predator–prey pattern, there is a time lag between the peak in phytoplankton density and zooplankton density (Figures 5 and A10). Note that higher, i.e., almost four times higher, zooplankton densities in the spring blooms were observed in the nearshore region as compared to the offshore region. In the nearshore region, the zooplankton density ranged from 0.002 to 0.41 $mmol\ N\ m^{-3}$ (Figure A7); in the mid- and offshore regions, these ranges were 0.003–0.12 $mmol\ N\ m^{-3}$ and 0.002–0.10 $mmol\ N\ m^{-3}$, respectively (Figure A7).

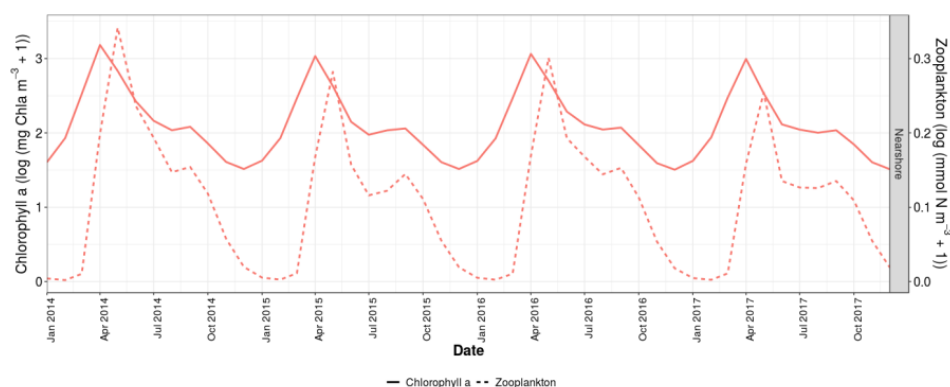


Figure 5. The phyto- (solid line) and zooplankton (dashed line) density simulations obtained via the nutrient–phytoplankton–zooplankton model in the nearshore region of the BPNS. The lines represent the average phyto- and zooplankton density predictions.

3.3. Relative Contributions

We found that solar irradiance and zooplankton grazing are the most important determinants of phytoplankton biomass throughout the year (Figure 6). Together they contribute 38% to 77% to the phytoplankton biomass dynamics in the BPNS. The contribution of zooplankton grazing is the highest after the spring blooms (31%) and during the autumn months (35%). PAR plays a more important role in the phytoplankton biomass during, autumn (43%). We found that the nutrients and SST play a relatively less important role in phytoplankton biomass dynamics. The total contribution of nutrients is, at maximum, 44%. During spring bloom, PO_4 plays an important role, while SiO_3 and DIN take over during early summer (Figure 6 and Appendix G). PO_4 is the most limiting nutrient (12–29%), followed by DIN (3.6–26%) and SiO_3 (1.2–15%), respectively. The SST only plays a limiting role during winter (max. 17%, Figure 6).

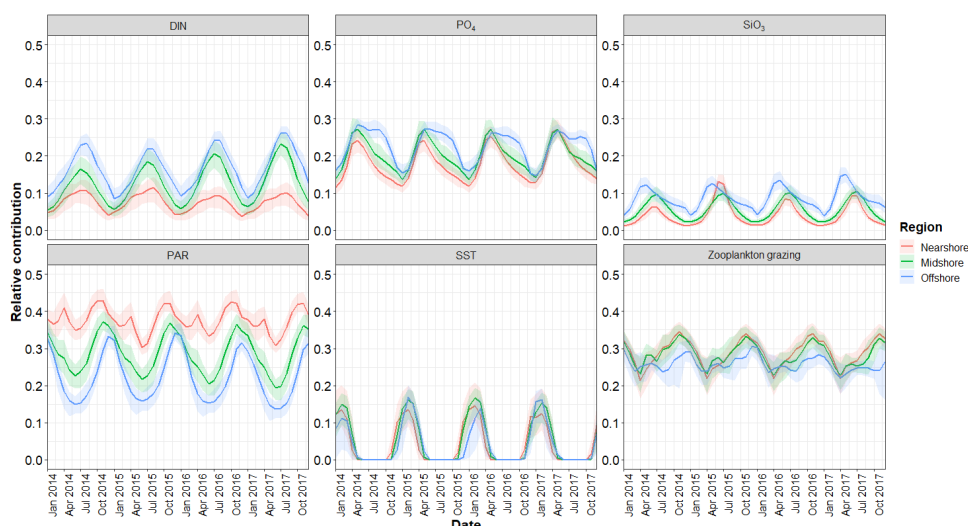


Figure 6. Monthly averaged relative contributions for each determinant of phytoplankton biomass dynamics for the three regions, i.e., nearshore, midshore, and offshore. The shaded areas indicate the 95% confidence interval. Potential determinants are dissolved inorganic nitrogen (DIN), phosphate (PO_4), silicate (SiO_3), solar irradiance (PAR), sea surface temperature (SST), and zooplankton grazing.

The relative contributions gradually changed along the nearshore–offshore transect (Figures 6 and 7). For example, the PAR’s relative contribution is the highest in the nearshore region (30–43%) and decreases towards the open sea (14–34%). Zooplankton grazing is less important in the offshore (22–31%) than in the nearshore region (21–35%) or the midshore region (23–34%). There is also a nearshore–offshore gradient in terms

of the relative contribution of nutrients (Figure 7). For each of the individual nutrients, i.e., DIN, PO_4 , and SiO_3 , we found them to be more limiting in the offshore region (8.5–26%; 15–29%; 3.9–15%, respectively) than in the nearshore region (3.7–11%; 12–27%; 1.2–13%, respectively). The SST was equally limiting in all three regions (Figure 7).

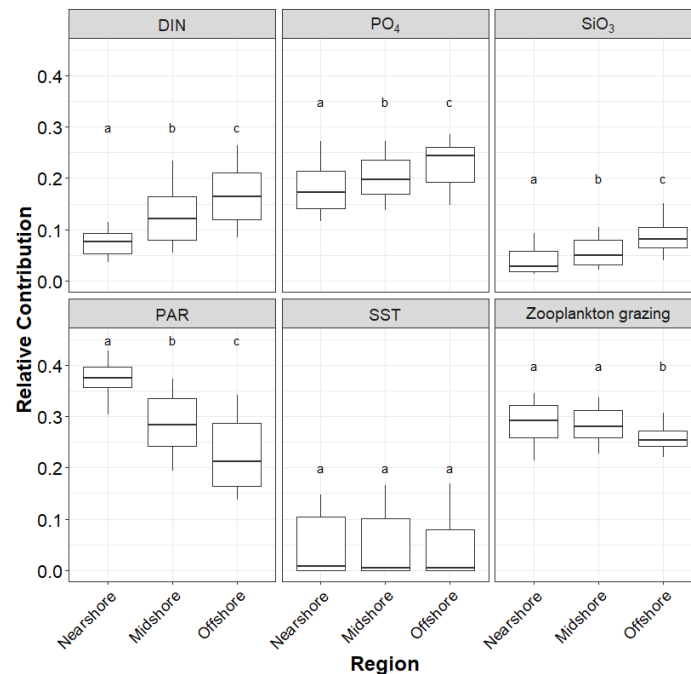


Figure 7. Monthly averaged relative contributions for each potential determinant of the phytoplankton biomass dynamics in the nearshore, midshore, and offshore regions. Statistically significant differences were set at $\alpha = 0.05$ between the regions, and are indicated by 'a', 'b', or 'c'. The potential determinants are dissolved inorganic nitrogen (DIN), phosphate (PO_4), silicate (SiO_3), solar irradiance (PAR), sea surface temperature (SST), and zooplankton grazing.

4. Discussion

Using an NPZ model, we reproduced phytoplankton and zooplankton dynamics in the BPNS (Figures 4 and 5), and we quantified the relative contribution of the key determinants of the phytoplankton biomass, i.e., the nutrients, solar irradiance, SST, and zooplankton grazing (Figures 6 and 7). This was conducted for three regions, i.e., the near-, mid-, and offshore, to examine the spatiotemporal variation. Only a few studies, e.g., Everaert et al. [12], Llope et al. [13], and McQuatters-Gollop et al. [14], have quantified the temporal relative contribution of phytoplankton biomass' key determinants. We found clear regional differences and seasonal patterns in the relative contribution of the key determinants of phytoplankton biomass dynamics.

4.1. Generalised Additive Modelling Performance

The GAMs were created based on the available monthly data and their model fit was assessed following the method of Zuur et al. [29]. Using monthly data meant that the performance of the models was restricted by the availability of data. Although the R^2 was not high, the smoothers created based on the GAMs captured the expected seasonality changes that were observed in the nutrient data. It was possible to capture the seasonality changes in the nutrient input data but within a reduced variance of the possible range for the input data. This could have affected our phytoplankton biomass dynamics if the nutrients were underestimated in the GAMs. Phytoplankton blooms may have been simulated smaller when the nutrient concentrations were estimated lower than they were in reality. This may have led to a flattening of the phytoplankton biomass dynamics, i.e., the extreme peak values may have been missed.

4.2. Comparison Phyto- and Zooplankton Modelling Results

The in situ chlorophyll-a concentrations of this study (nearshore: 1.1–57.5 mg Chla m⁻³, midshore: 0.6–13.1 mg Chla m⁻³, and offshore: 0.2–10.3 mg Chla m⁻³) were close to other field studies in the BPNS (Figure 8), such as Desmit et al. [9] (nearshore: 1–20 mg Chla m⁻³, and offshore: 0.5–15 mg Chla m⁻³) and Muylaert et al. [48] (nearshore: 0.2–60 mg Chla m⁻³, midshore: 0.2–20 mg Chla m⁻³, and offshore: 0.2–15 mg Chla m⁻³). The NPZ model predictions (nearshore: 3.5–23.1 mg Chla m⁻³, midshore: 1.8–8.8 mg Chla m⁻³, and offshore: 1.4–5.3 mg Chla m⁻³) based on the chlorophyll-a concentrations observed in this study are close to the modelling results of Arndt et al. [8] (0.5–40 mg Chla m⁻³) and Lancelot et al. [49] (0.3–23 mg Chla m⁻³; Figure 8). However, our model predictions did not show extreme, i.e., high and/or low, phytoplankton densities, thus resulting in the phytoplankton biomass predictions being close to the modelled-based quantifications found in the literature (Figure 8). In neighbouring regions, similar chlorophyll-a values were observed by, e.g., Alvarez-Fernandez et al. [50], Lancelot et al. [49], EEA [51], Colella et al. [52], and Lundsør et al. [53] (Figure 8). Although the chlorophyll-a concentrations are in line with previous studies, we noticed that there is some variability between previous studies and our observations. A potential reason for this is that the data used in this study are more recent. Indeed, with the inclusion of recent observations, Desmit et al. [9] found a decrease in the annual mean chlorophyll concentration for offshore regions over a time span of 40 years. This is supported by Xu et al. [54], thereby demonstrating a decreasing trend in the chlorophyll-a in the offshore region of the central North Sea.

In the BPNS, our model indicated a clear seasonal pattern with low phytoplankton biomass in winter (min. 1.4 mg Chla m⁻³) and increasing phytoplankton biomass during spring. This spring bloom (max. 23.1 mg Chla m⁻³), typically consisting of diatoms and *Phaeocystis* spp. [48], occurs in March and April and is followed by a smaller bloom in autumn (max. 7.7 mg Chla m⁻³). We found a decrease in phytoplankton biomass overall, and a decrease of the amplitude of the spring bloom (23.1 mg Chla m⁻³ nearshore to 5.3 mg Chla m⁻³ offshore) with increasing distances from the coast (Figure 4). These regional differences were also observed by Desmit et al. [9] (20 mg Chla m⁻³ nearshore to 12 mg Chla m⁻³ offshore) and Muylaert et al. [48] (60 mg Chla m⁻³ nearshore to 15 mg Chla m⁻³ offshore) in the BPNS. Muylaert et al. [48] and Desmit et al. [9] have also observed that the seasonal pattern, i.e., a spring bloom followed by a smaller autumn bloom, was more distinct when closer to the coast (Figure 4). Jiang et al. [55] found a high interannual variability in the peak biomass, which is also observed in our field observations but is less expressed in our modelling results. Nevertheless, in nearshore regions we see that the autumn bloom is more modest, i.e., three to four times smaller in amplitude, than the spring bloom.

The classic bimodal bloom pattern that we (Figure 5) and others (e.g., Muylaert et al. [48] and Lancelot et al. [49]) have observed in the BPNS was not found by Nohe et al. [56] between 2003 and 2010. They found that the spring bloom was more intense and extended, and that there was no autumn bloom. Nohe et al. [56] suggested that increased SST and water transparency, as well as changes in nutrient concentrations and ratios, are potential reasons for the lack of an autumn bloom. This lack of an autumn bloom is in strong contrast with our findings with more recent data, i.e., 2014–2017. Similar to our study, Speeckaert et al. [57] found two blooms, i.e., a spring bloom followed by a smaller autumn bloom in 2016, whereas Nohe et al. [56] observed a mean diatom cell density of 3.9×10^5 cell L⁻¹ in the autumns in the period of 2003–2010. In addition, Speeckaert et al. [57] found a peak cell density of 2.0×10^6 cell L⁻¹ with *Guinardia* spp., which is the dominant diatom in the autumn bloom in 2016. This autumn bloom is also observed in the data from the LifeWatch Flowcam [58,59] for 2017 and later (Figures A12–A14). This suggests that the BPNS may have shifted back to a two-bloom pattern.

The seasonal dynamics of zooplankton correspond largely with the data found by van Ginderdeuren et al. [27], Mortelmans et al. [24], and Deschutter et al. [60] for copepods, which largely dominate the zooplankton community in the BPNS [27,61]. The delayed

increase in zooplankton density corresponding with the spring bloom, illustrating the zooplankton grazing on phytoplankton in our model (Figures 5 and A10 [49]), depicts the population dynamics of a classic predator–prey relationship [62]. Zooplankton grazing is an important determinant of phytoplankton biomass dynamics, but the predator–prey relationship is complex and changes under different abiotic conditions [63].

The LifeWatch observations and our model results suggest higher zooplankton density in nearshore regions (Figure 4), and this agrees well with the findings of Mortelmans et al. [64] and of Deschutter et al. [60] for the BPNS. This was also observed in other areas in the world [65,66]. Van Ginderdeuren et al. [27] observed that the highest copepod densities occurred in their ‘midshore region’ of the BPNS, but that region overlaps with our nearshore region (Figure 1).

4.3. Relative Contribution of the Key Determinants

This study provides a better understanding on the spatiotemporal variation in the relative contribution of the key determinants of marine phytoplankton biomass dynamics in the BPNS through using an NPZ model that is driven by in situ observation. The relative contributions of key determinants to changes in the phytoplankton biomass dynamics are highly seasonal and spatially related in the BPNS.

The relative contribution of the determinants changes seasonally (Figure 6). During autumn and winter, when there is the least amount of light in the BPNS (± 8 h per day), the PAR is the major determinant (max. 43%). Obviously, sufficient solar irradiance is needed for photosynthesis [67]. The SST becomes more of a limiting factor for phytoplankton growth during mid-winter and early spring (max. 17%). This was also found by Everaert et al. [12]. They found that the combined relative contribution of the SST and PAR varied from 20% during summer to 50% during winter, which is similar to our results (summer: 14% and winter: 51%). In shallow coastal areas like the BPNS, the SST is a key factor affecting phytoplankton bloom dynamics [68] as the low temperature decreases the growth rate of marine phytoplankton [69]. In early spring, when solar irradiance and temperature increases, phosphorus becomes depleted due to the spring bloom [8,49,70] and becomes the major determining factor (29%). Nitrogen becomes increasingly limiting in early summer (26%), together with silica in the nearshore (13%) and midshore (10%) regions. The increased phytoplankton density during spring bloom results in a higher zooplankton density after the spring bloom in early May [64]. Together with zooplankton density, the grazing pressure on phytoplankton increases. During summer and autumn, zooplankton grazing is an important determinant with a high relative contribution on the phytoplankton biomass (31% and 35%, respectively); this is because zooplankton biomass remains high [64], whereas phytoplankton biomass decreases, thus changing the phytoplankton–zooplankton ratio. This corresponds with the findings of Gowen et al. [71] for the Irish Sea, who found that the percentage of phytoplankton biomass grazing is highest after spring bloom in May. From the winter onwards, zooplankton grazing’s relative contribution decreases as their abundance has decreased together with their food supply, i.e., phytoplankton, which is mainly limited again by the low solar irradiance completing the seasonal cycle of the determinants (Figure 6).

Besides their temporal variability (cfr. previous paragraph), the key determinants affecting phytoplankton biomass also vary spatially. The influence of nutrients on the phytoplankton biomass dynamics increases with increasing distance from the coastline (Figure 7). The main reason for this is related to the fact that nearshore regions tend to be nutrient-rich due to riverine discharges. As the river runoff creates a nearshore–offshore gradient in nutrients with lower nutrient availabilities in offshore regions (Figure A4, [8,70]), all nutrients have a higher relative contribution in limiting phytoplankton biomass (Figures 6 and 7), i.e., nitrogen (8.5–26%), phosphorus (15–29%), and silica (3.9–15%). The difference in relative contributions between nearshore and offshore regions is most obvious for nitrogen, i.e., DIN is being more limiting in the offshore region (max. 26%) than in the nearshore (max. 11%) region. Phosphorus, on the other hand, limits phytoplankton biomass in the

offshore region for a longer period. This could be related to the water depth as phosphorus is largely regenerated from the sediment; additionally, for the offshore region, there is a much higher water mass-to-sediment ratio [70]. Silica becomes a limiting factor earlier in the offshore region than in the near- and midshore regions, as the low SiO₃ reserve in the offshore region is depleted quickly during the spring bloom [48]. The gross part of riverine nutrient resources (the Scheldt, Rhine, Meuse, and Seine [18]) is depleted before it reaches the offshore region [8]. Our results largely agree with the findings of Burson et al. [72], i.e., nearshore regions in the North Sea are P limited and, the mid- and offshore regions of the BPNS are N and P co-limited. The impact of zooplankton grazing on phytoplankton biomass is smaller in offshore regions, which could be due to the lower zooplankton density (Figure A7), and thus the lower grazing pressure. In the nearshore region, PAR is a major determinant year-round (30–43%); whereas, in the mid- and offshore regions (14–34%), this is more in balance with the other determinants (Figure 7). The high turbidity in the nearshore region [18,73] restricts the phytoplankton’s access to sunlight and causes PAR to be a major determining factor throughout the year. The more offshore the region, the less influential PAR is in terms of phytoplankton biomass dynamics.

Overall, the relative contributions of the key determinants of phytoplankton biomass dynamics showed a clear spatiotemporal variation. The spatiotemporal variation is partially driven by meteorological conditions, which affects currents, temperature, the levels of SPM, light availability, river discharge, and nutrient dynamics in the BPNS [74]. Nutrients from various rivers such as the Seine and Somme are carried by the influx of Atlantic water to the BPNS [18]. Local rivers, primarily the Scheldt, Rhine, and Meuse—which flow through industrialised and densely populated areas, thus providing them with high nutrient loads—further contribute to the nutrient status of the BPNS [75]. Consequently, there is a noticeable southeast–northwest gradient in nutrient concentrations, which was also observed in the relative contributions of the nutrients (Figures 6 and 7). Similar to the nutrient gradient, a salinity gradient from east to west is created due to the Scheldt [16]. The BPNS also exhibits a gradient in PAR, primarily due to spatial variations in the SPM and in the dissolved organic matter. In the vicinity of the coastline, shallow waters tend to be more turbid and have higher SPM concentrations [75,76]. These factors mainly drive the spatial gradient in phytoplankton biomass dynamics (Figure 4) in the BPNS.

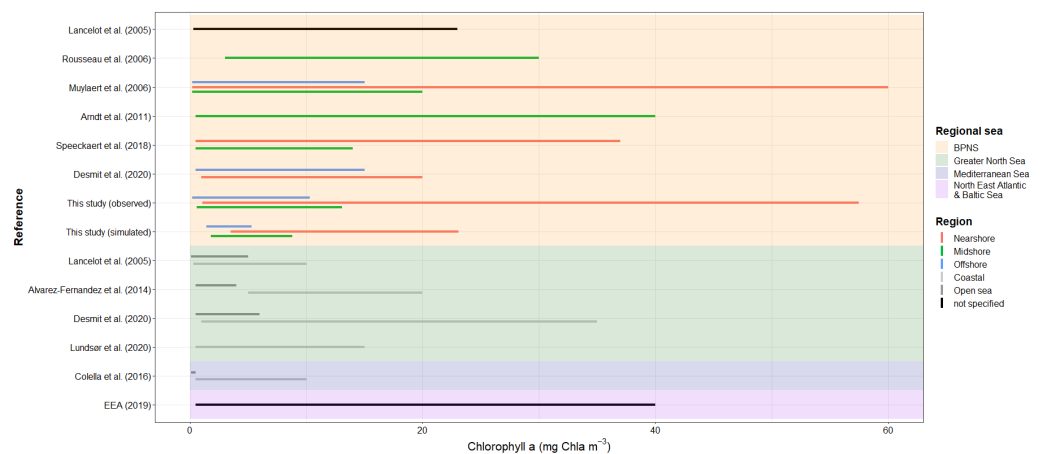


Figure 8. An overview of the phytoplankton biomass concentrations in the Belgian part of the North Sea (BPNS, yellow) [8,9,48,49,57,76], Greater North Sea (green) [9,49,50,53], Mediterranean Sea (blue) [52], and the North East Atlantic and Baltic Sea (purple) [51]. The phytoplankton biomass concentrations are subdivided by region, the near-, mid-, and offshore regions in the BPNS, as well as the coastal and open sea regions in the Greater North Sea, Mediterranean Sea, and North East Atlantic and Baltic Sea. Citations on the y-axis refer to the corresponding studies. For the present study, both model-based simulated phytoplankton biomass (This study (simulated)), as well as in situ observations (This study (observed)) have been integrated.

Whereas the temporal variation in phytoplankton biomass, i.e., the blooms (Figure 4), are mainly determined by temperature and PAR (Figure 6) [63]. Increased temperature resulting from more solar irradiation promotes phytoplankton growth. Additionally, the increased settling of SPM in spring increases the light availability. The temporal changes in PAR are influenced by the resuspension and movement of particulate matter, which are further modified by winds and tides. For example, the stronger winds during winter lead to a higher attenuation of PAR. This settling process affects the timing of the onset of spring phytoplankton blooms [75,76].

The temporal variation in phytoplankton biomass is also, to a lesser extent, determined by the mixing of the water column, nutrient conditions, grazing, and phytoplankton community composition [63]. For example, in most areas of the region, the BPNS exhibits a constant mixing of the water column throughout the year due to a combination of robust tidal currents and shallow depth [15,77].

Additionally, there are also factors that could affect the phytoplankton biomass dynamics, such as anthropogenic activities [78–82] and biological agents [83–85]. Biological agents, such as bacteria and viruses can affect the bloom development and termination [83,85]. For example, the rapid proliferation of viruses can have a strong influence on the populations of phytoplankton hosts, thus playing a crucial role in marine biogeochemistry and ecology [83].

Quantifying the relative contribution and identifying the spatiotemporal variation offer a better understanding of how the key determinants' limitations to phytoplankton biomass will change under changing conditions, e.g., those related to climate change. However, every method has its advantages and limitations, and below we consider those of our modelling approach before addressing the potential implications of this study.

4.4. Modelling with Field Data: Advantages and Limitations

Often multiple driver-related research has been performed in laboratories. A big advantage of this is that model species can be kept in optimal conditions, e.g., temperature, light, nutrients, etc., which aids in isolating the effects of the stressor in question. However, these optimal conditions are rarely experienced by organisms in their natural environment [86], thus hampering the conversion of the laboratory-based conclusions towards field conditions. Therefore, we have selected a modelling approach using field data, which has the advantage that the natural background variation of bottom-up drivers of marine ecosystems are implicitly included in the results [87]. Therefore, by using field data to quantify the relative contribution, we can assess the impact of the determinants under their natural and continuously changing conditions.

Even though the phytoplankton biomass dynamics modelled in this study agree well with the field observations from LifeWatch (Figure 4), we acknowledge that our modelling approach contains limitations: (i) The periods with low phytoplankton growth in the offshore region correspond less with the field observations. This is likely attributable to the seasonal sampling strategy in that region, i.e., no monthly measurements [23]. As such, we had less data available for the offshore region to calibrate our model. (ii) In this study, only one station, i.e., station 130, for the nearshore region, and one station, i.e., 330, for the midshore region were selected to represent their region. Data exploration on the publicly accessible LifeWatch server shows that the patterns seen in the data from station 130, chosen to represent the nearshore area, were also evident in the data from other nearshore stations, such as station 120 in the west and station 700 in the east. This conclusion also applies to the midshore region, currently represented by station 330, as similar dynamics were found in station ZG02 and station W07bis. (iii) For the NPZ model, different functional groups of phytoplankton and zooplankton were grouped, and—by doing so—we may have missed species-specific limitations. It is known that reactions to changes in determinants, such as with climatic changes, are quite species-specific [88,89]. (iv) Additionally, only the most abundant and dominant zooplankton species, i.e., copepods and Appendicularia, were aggregated. However, they account for 76% of the total zooplankton density [27],

and, as such, represent the main biomass dynamics of zooplankton. (v) Chl:N ratios are known to have a seasonal trend [90]. This seasonality was accounted for by selecting two Chl:N ratios, i.e., one ratio to reflect spring conditions and one ratio for autumn conditions. These ranges were selected based on minimising the RMSE for each season. As such, after calibration, model simulations were performed on fixed Chl:N ratios for each season. Using the fixed Chl:N ratios could have caused a flattening of the curve, in both high (spring bloom peak) and low (in winter) extreme values in phytoplankton densities. Even though Chl:N ratios were selected for each region individually, the pattern of over- (during winter) and underestimating (during spring) was found at each region (Figure A5). The over- (during winter) and underestimating (during spring) was most pronounced in the nearshore region (Figure A5). Additionally, the overestimation of phytoplankton density at low observed densities, i.e., in winter (Figure A5), may have resulted from the selected Chl:N ratio for the autumn conditions (Table 1) (which was in the upper part of the range found in the literature (Table A1)). (vi) The NPZ model does not include a horizontal and vertical mixing of the nutrients in the water column. Nevertheless, these were accounted for: firstly, the BPNS is permanently mixed [16]; and secondly, the model was calibrated and fitted using in situ observations, which contain vertical and horizontal mixing characteristics [23]. However, when the model would be applied to another area where stratification does occur, vertical and horizontal mixing should be accounted for. (vii) Using a fixed sinusoidal surface irradiance in our small study area, i.e., 67 km to 65 km, did not impact our calculations as the difference on such a small scale is negligible. When applying the model to large areas, the spatial properties of this factor should be considered.

Although other coastal and regional sea models exist for the North Sea, e.g., ERSEM, MIRO, and ECOHAM [49,91,92], we used the NPZ model to make the best use of the LifeWatch datasets. The complexity of the aforementioned models was not suited for our goal, that is, to develop a model to assess which factors drive marine phytoplankton biomass dynamics in the BPNS and how their relationship to primary production varies on a spatiotemporal scale.

Using this NPZ model allowed us to integrate and simulate with forcing functions. In turn, integrating the forcing functions gave us the possibility to determine the relative contributions, and it permits us to add forcing functions in the model. In addition, this NPZ model can be applied on a small scale, which is needed as the difference in the parameterisation of the regions (Table 1) illustrate. Models covering larger areas produce more general patterns. These general patterns have less detailed information on local differences that is required to enable policymakers to make local decisions. We provided here the first step towards such a model that adheres to the need to understand the consequences of blue economy investments in the BPNS. An advantage of the NPZ model, being less complex, is that it requires less computing power and time.

In addition, some components, e.g., the vertical mixing and depth levels, which are included in the more complex models such as ERSEM [91], are less applicable to the BPNS. The BPNS is permanently mixed [16], and photosynthesis is restricted to the top layer as available light usually does not penetrate the water column more than ten meters [93]. More complex models can provide a more detailed and comprehensive set of outputs than NPZD models as they include a wider range of physical, chemical, and biological variables. However, this could also make it more complex for the end users, such as industry workers and policymakers, to interpret and analyse the model results. Overall, using an NPZ model was selected as the optimum between computing time, interpretability, and complexity in terms of addressing our research topic.

The novelty of this study lies in five aspects: (1) performing a high-resolution spatiotemporal analysis that contributes to a better understanding of phytoplankton biomass dynamics in the BPNS (cfr. 4.2), (2) quantifying the relative contribution of the determinants of phytoplankton biomass dynamics along a near-offshore gradient (cfr. 4.3), and (3) the observation of a bimodal bloom pattern in the BPNS after being absent from 2003 until 2010 (cfr. 4.2). Furthermore, this study has the potential to support dedicated management

strategies for a sustainable development of Belgium's blue economy (see Section 4.5). Finally, as the fifth aspect, the modelling scripts and data are available according to the FAIR principles (see Data Availability Statement Section).

4.5. Future Perspectives and Implications

Our model is well suited to simulating local phyto- and zooplankton dynamics, and it could be used to complete data gaps in phytoplankton and zooplankton observations. Upon the availability of abiotic input variables, these abiotic input variables could be used to drive the model to obtain phytoplankton and zooplankton biomass, thus completing the data gaps. The obtained results should be validated with the available observations from before and after the data gap. In addition, our model and results could be used to evaluate how the key drivers of phytoplankton biomass change under climate change conditions and blue economy activities. As such, this model is suitable for understanding and predicting the consequences of compound events, which are defined as and generated by short time changes (weather related) combined with climate events [94].

During the Anthropocene, human activities have caused ocean warming [96], acidification [95], and eutrophication [96], resulting in an on-average increasing SST, and increased nutrient concentrations compared to the pre-industrial times. To date, it is not clear which long-term changes in abiotic conditions are most important in the context of marine phytoplankton biomass dynamics. It is hypothesised that the relative contribution of the dominant determinants will change due to changing environmental conditions [97]. Modelling and quantifying the relative contribution of the phytoplankton's determinants provide a more holistic view rather than a one-to-one relation that is obtained from directly measuring phytoplankton biomass. The quantification of relative contribution could give more insight into the underlying mechanisms, e.g., changes in the relative contribution of the key determinants of phytoplankton biomass may indicate a disruption of the phytoplankton community [98,99]. Modelling climate change scenarios should always be performed carefully as (i) the NPZ model does not include different species and could miss changes in the community composition, e.g., due to a poleward shift [98], and (ii) the natural variability of the phytoplankton dynamics may not be fully covered in the four years analysed in this study [100].

In the context of the blue economy, our model contributes to a better understanding and quantification of the dynamics of the local ecosystem and the potential effects of human activities on the marine environment. Here, we present two concrete blue economy cases in which the model can be used to assess the potential consequences of aquaculture development and wind farms on the local ecosystem. In the case of bivalve aquaculture, it is anticipated that nutrient fluxes will be adapted through bottom-up effects [78,79], as well as the limitation of phytoplankton production through filter feeding [80,81]. Once a wind farm is operational, a well-known effect that is generated is the turbidity plume [82]. The decrease in light availability may lead to a decrease in phytoplankton productivity locally. These changes in abiotic conditions can be translated via the NPZ model to phytoplankton biomass dynamics. Overall, our model has the potential to evaluate the effectiveness of various management strategies while being less complex, which could translate to it being user friendly and having more users, e.g., scientists and policymakers.

The model could benefit from (i) using different sources for validation, (ii) expanding the scope of the model, and (iii) by incorporating a greater amount and more accurate data. Firstly, for the validation of the model, high-resolution remote sensing data could be used. This would work well with climate change conditions [101]. Secondly, based on the results of this local model, it would be possible to integrate more parameters, and more complexity could also be built, such as hydrodynamics. This is conducted, for example, in the ERSEM and MIRO models, where the NPZD model is incorporated into a complex model. Lastly, we provided the first step in this direction with our NPZ model, which has the potential to be further developed to a more detailed taxonomical level, e.g., using CHEMTAX as this allocates chlorophyll-a to phytoplankton groups by marker pigments

and Chla ratios [102–104]. It would also be possible to include, in a further iteration, more detailed data, e.g., data on a more detailed taxonomic level, to have a better understanding of the effects of each of the key determinants on the various subgroups of phytoplankton to predict whether the ecosystem will change [105] (even though phytoplankton biomass dynamics are resilient to a certain extent [106]).

5. Conclusions

In this study, a first step towards a model that adheres to the need to understand the consequences of blue economy investments in the BPNS, is provided. We quantified phytoplankton biomass dynamics and the relative contribution of its determinants using an NPZ model along a near-offshore gradient over a period of four years (2014–2017). By doing so, a better understanding of the spatiotemporal variations in these contributions was provided. After not being observed between 2003 and 2010, we again found a classic bimodal bloom pattern. Further, we found that the relative contributions of phytoplankton determinants alter spatially and temporally. Solar irradiance (up to 43%) and zooplankton grazing (up to 35%) are the most influential determinants for phytoplankton biomass, and this is the case throughout the year. A clear spatial gradient was observed for most of the determinants, e.g., nutrients and zooplankton grazing, which are greater limiting factors offshore, while the opposite is true for solar irradiance. This comprehensive study contributes to a better understanding of phytoplankton biomass dynamics and its determinants along a near-offshore gradient in the BPNS. Additionally, it has the potential to support blue economy strategies and management in the BPNS. In the scope of future climate scenarios and blue economy, it is important to understand the key determinants of phytoplankton biomass dynamics to develop management scenarios that ensure a sustainable marine ecosystem.

Author Contributions: V.O.: Conceptualisation, Methodology, Software, Validation, Investigation, Data Curation, Writing—Original Draft, Writing—Review and Editing. S.P.: Software, Validation, Formal analysis, Writing—Original Draft, Writing—Review and Editing, Visualisation. K.D.: Writing—Review and Editing. M.D.R.: Writing—Review and Editing. J.M.: Investigation, Writing—Review and Editing. L.S.: Writing—Review and Editing. P.M.-C.: Writing—Review and Editing, Project administration. K.S.: Writing—Review and Editing. W.V.: Writing—Review and Editing. M.V.: Writing—Review and Editing. G.E.: Conceptualisation, Methodology, Writing—Review and Editing, Supervision. All authors have read and agreed to the published version of the manuscript.

Funding: This work was supported by the European Union’s Horizon programme—H2020 Blue-Cloud project (grant number 862409) (for V.O., S.P., and P.M.-C.) and the European Union’s Horizon Europe research and innovation programme—Blue-Cloud 2026 project (grant number 101094227) (for S.P. and P.M.-C.). L.S. was supported by the Research Foundation—Flanders (FWO) as part of the Belgian contribution to LifeWatch (I002021N-LIFEWATCH).

Institutional Review Board Statement: Not applicable.

Informed Consent Statement: Not applicable.

Data Availability Statement: The results reported in this manuscript have been obtained by using a dedicated working environment: Zoo and Phytoplankton EOVS Products Virtual Laboratory operated by D4Science.org (https://blue-cloud.d4science.org/web/zoo-phytoplankton_eov, accessed on 15 March 2023). This working environment hosts the data and the software, thus making the process leading to the results repeatable according to open science practices. The processed data and scripts have also been published in the Blue-Cloud Catalogue (https://data.d4science.org/ctlg/Zoo-Phytoplankton_EOV/spatiotemporal_analysis_of_plankton_drivers_in_the_belgian_part_of_the_north_sea_data, accessed on 10 March 2023), as well as deposited in Zenodo (<https://doi.org/10.5281/zenodo.6794084>, accessed on 10 March 2023) under a Creative Commons CC-BY 4.0 license. This allows for the use of the data and code under the condition of providing the reference to the original source: Steven Pint and Viviana Otero (2021). Data, scripts, and model output to perform spatiotemporal analysis of the plankton drivers in the Belgian part of the North Sea (dataset). Zenodo: <https://doi.org/10.5281/zenodo.6794084>, accessed on 10 March 2023. The raw input data

that was obtained from LifeWatch can be accessed through <https://doi.org/10.14284/441> and <https://doi.org/10.14284/445>, accessed on 10 March 2023, or via <https://rshiny.lifewatch.be/>, accessed on 10 March 2023.

Acknowledgments: The production of this work has been supported by the Blue Cloud working environment via the Blue Cloud (<https://blue-cloud.d4science.org>, accessed on 15 March 2023) operated by D4Science.org (www.d4science.org, accessed on 15 March 2023) [107]. This work makes use of the LifeWatch data and infrastructure funded by Research Foundation—Flanders (FWO) as part of the Belgian contribution to LifeWatch ESFRI.

Conflicts of Interest: The authors declare no conflict of interest.

Appendix A. NPZD Model Parameters

The initial values of the model for phytoplankton ($1.0 \text{ mmol N m}^{-3}$), zooplankton ($0.1 \text{ mmol N m}^{-3}$), and DIN ($5.0 \text{ mmol N m}^{-3}$) were taken from Soetaert and Herman [19].

Table A1. Parameterisations of the nutrient–phytoplankton–zooplankton (NPZ) model, i.e., the minimum and maximum values, units, and references. These intervals are used as a reference to create the different sets to calibrate the NPZ model. * Minimum and maximum values for k_d were calculated for each region of interest based on CTD data recorded in MIDAS.

Parameter	Minimum Possible Value	Maximum Possible Value	References
maxUptake	0.25 (day^{-1})	1.5 (day^{-1})	[19,108–111]
excretionRate	0.1 (day^{-1})	0.2 (day^{-1})	[19,109,111]
maxGrazing	0.8 (day^{-1})	1 (day^{-1})	[19,108,109,112,113]
k_{SGrazing}	1 (mmol N m^{-3})	4 (mmol N m^{-3})	[19,113,114]
pFaeces	0.2 (day^{-1})	0.5 (day^{-1})	[19]
mortalityRate	0.25 ($(\text{mmol N m}^{-3})^{-1} \text{ day}^{-1}$)	0.5 ($(\text{mmol N m}^{-3})^{-1} \text{ day}^{-1}$)	[19,108–111,113,115]
ChlNratio	1 (mg Chla/mmol N)	8 (mg Chla/mmol N)	[50]
k_{SPAR}	30 ($\mu\text{Einst m}^{-2} \text{ s}^{-1}$)	250 ($\mu\text{Einst m}^{-2} \text{ s}^{-1}$)	[19]
T_{obs}	7 °C	15 °C	[8,113,114]
k_{SDIN}	0.25 (mmol N m^{-3})	5 (mmol N m^{-3})	[8,19,108–115]
k_{SP}	0.2 (mmol P m^{-3})	0.5 (mmol P m^{-3})	[8,113]
k_{SSi}	0.2 (mmol Si m^{-3})	0.8 (mmol Si m^{-3})	[49]
K_d *	0.6 (m^{-1})	1 (m^{-1})	Nearshore station
	0.27	0.67	Midshore station
	0.21	0.44	Offshore stations

Table A2. Root mean square error (RMSE) for each of the regions of interest based on the second iteration, whereby the 10% best simulations correspond to the number of simulations indicated in the last column. Each region of interest has a different number of best simulations as some of the combinations of the set of parameters resulted in exponential behaviour. Only the simulations that converged were considered to be the 10% best (i.e., lowest RMSE) out of the 5000 possible simulations.

Region of Interest	RMSE–Median (Q1–Q3)	Number of Simulations
Nearshore region	1.34 (1.32–1.36)	259
Midshore region	0.44 (0.43–0.45)	498
Offshore region	0.40 (0.37–0.41)	499

Table A3. The number of observations available of Chlorophyll-a and zooplankton densities for the nearshore, midshore, and offshore regions (Figure 1) from 2014 to 2017.

Variable	Nearshore Region	Midshore Region	Offshore Region
Chlorophyll-a	39	37	98
Zooplankton	40	37	96

Appendix B. Zooplankton Conversion

The most common zooplankton found in the Belgian part of the North Sea (BPNS) are copepods [27]. The most common species are *Acartia clausi*, *Temora longicornis*, *Paracalanus parvus*, *Centropages hamatus*, *Pseudocalanus elongatus*, *Centropages typicus*, *Calanus helgolandicus*, and *Euterpina acutifrons* [27]. The dinoflagellate *Noctiluca scintillans* were also seasonally found in high densities, and Appendicularia *Oikopleura dioica* was found year round [27]. Therefore, the taxa Calanoida, Noctiluca, Harpacticoida, and Appendicularia were selected from the LifeWatch database to calculate the zooplankton abundance (ind m^{-3}).

The body mass per individual of each taxon was defined based on the most common species of each group (Table A4). The body mass per individual was calculated as the median value of body mass (mg C ind^{-1}) for the most common species of each taxon. Afterwards, the body mass in carbon was converted to mmol C by dividing by the molecular weight of C (12.0107 gr/mole). Finally, the mmol C m^{-3} is converted to mmol N m^{-3} based on the C:N ratio of each taxon (Table A5).

Table A4. The body mass per individual (mg C ind^{-1}) of the most common species of taxa found in the Belgian part of the North Sea.

Taxon	Body Mass (mg C ind^{-1})	Species	Reference
Calanoida	0.0006	<i>Acartia clausi</i> , <i>Temora longicornis</i> , <i>Paracalanus parvus</i> , <i>Centropages hamatus</i> , <i>Pseudocalanus elongatus</i> , <i>Centropages typicus</i> and <i>Calanus helgolandicus</i>	[116]
Noctiluca	0.0003	<i>Noctiluca scintillans</i>	[117]
Harpacticoida	0.001	<i>Euterpina acutifrons</i>	[118]
Appendicularia	0.002 to 0.006	<i>Oikopleura dioica</i>	[119]

Table A5. The C:N ratio for each of the most common taxa present in the Belgian part of the North Sea.

Taxon	C:N Ratio	Species	Reference
Calanoida	5.5–7	<i>Acartia</i> spp., <i>Temora</i> sp., <i>Centropages</i> , <i>Oithona</i> sp., <i>Pseudo/Paracalanus</i> spp.	[120]
Noctiluca	2.3–4.4	<i>Noctiluca scintillans</i>	[121]
Harpacticoida	4.26–4.74 7.7–8.1	<i>Euterpina acutifrons</i>	[122] [123]
Appendicularia	4.08	<i>Oikopleura dioica</i>	[119]

Appendix C. Smoothers for the Generalised Additive Models (GAMs) in the Three Regions of Interest, i.e., the Near-, Mid- and Offshore Regions

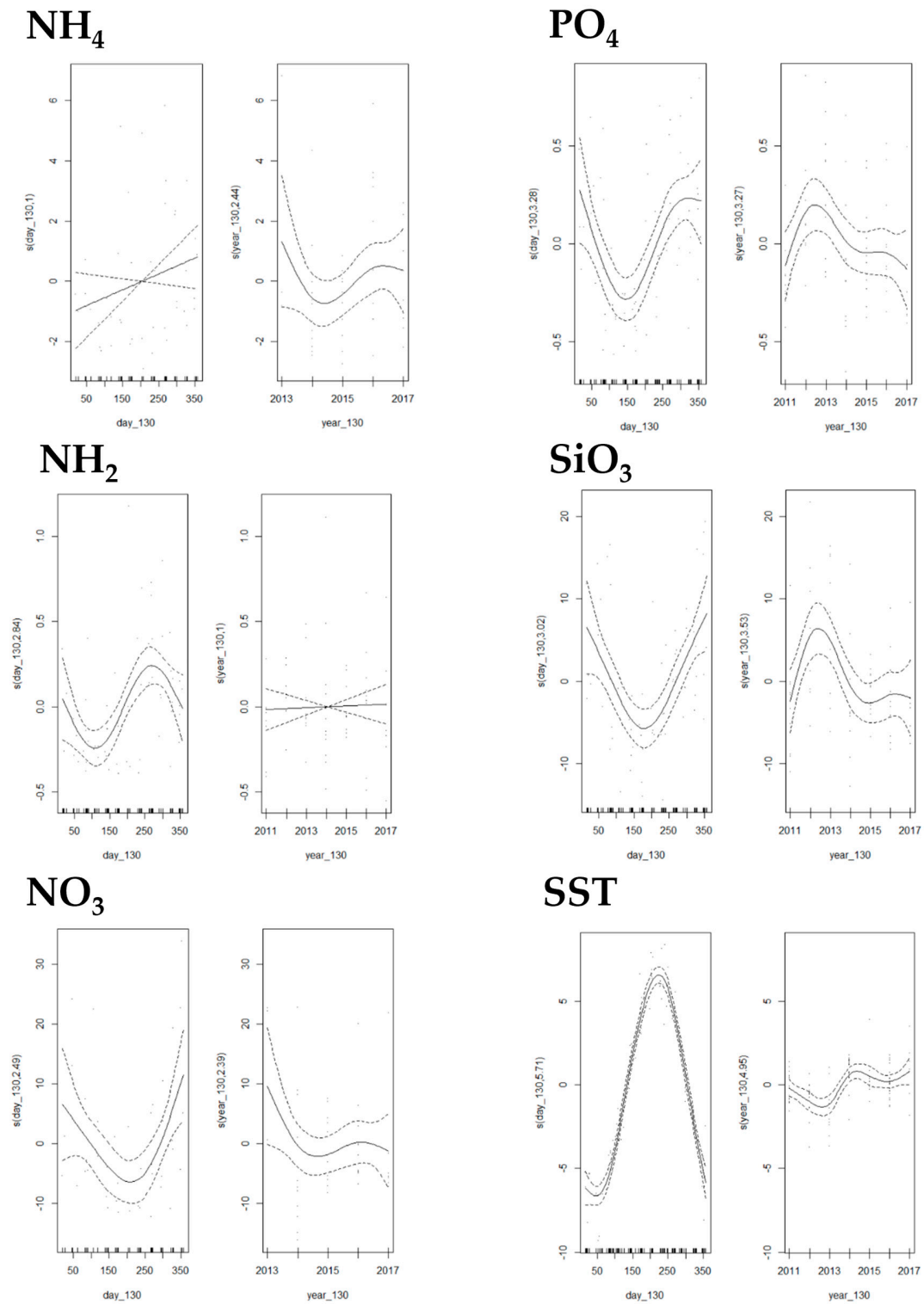


Figure A1. Smoothers for the day and year input variables, i.e., ammonium (NH_4), phosphate (PO_4), nitrite (NO_2), silicate (SiO_3), nitrate (NO_3), and the sea surface temperature (SST), for the generalised additive models in the nearshore region. The smoothers are calculated from 2011 to 2017 as the three first years are used as dummy years. The solid line represents the mean value, and the dashed lines are the 95% confidence interval.

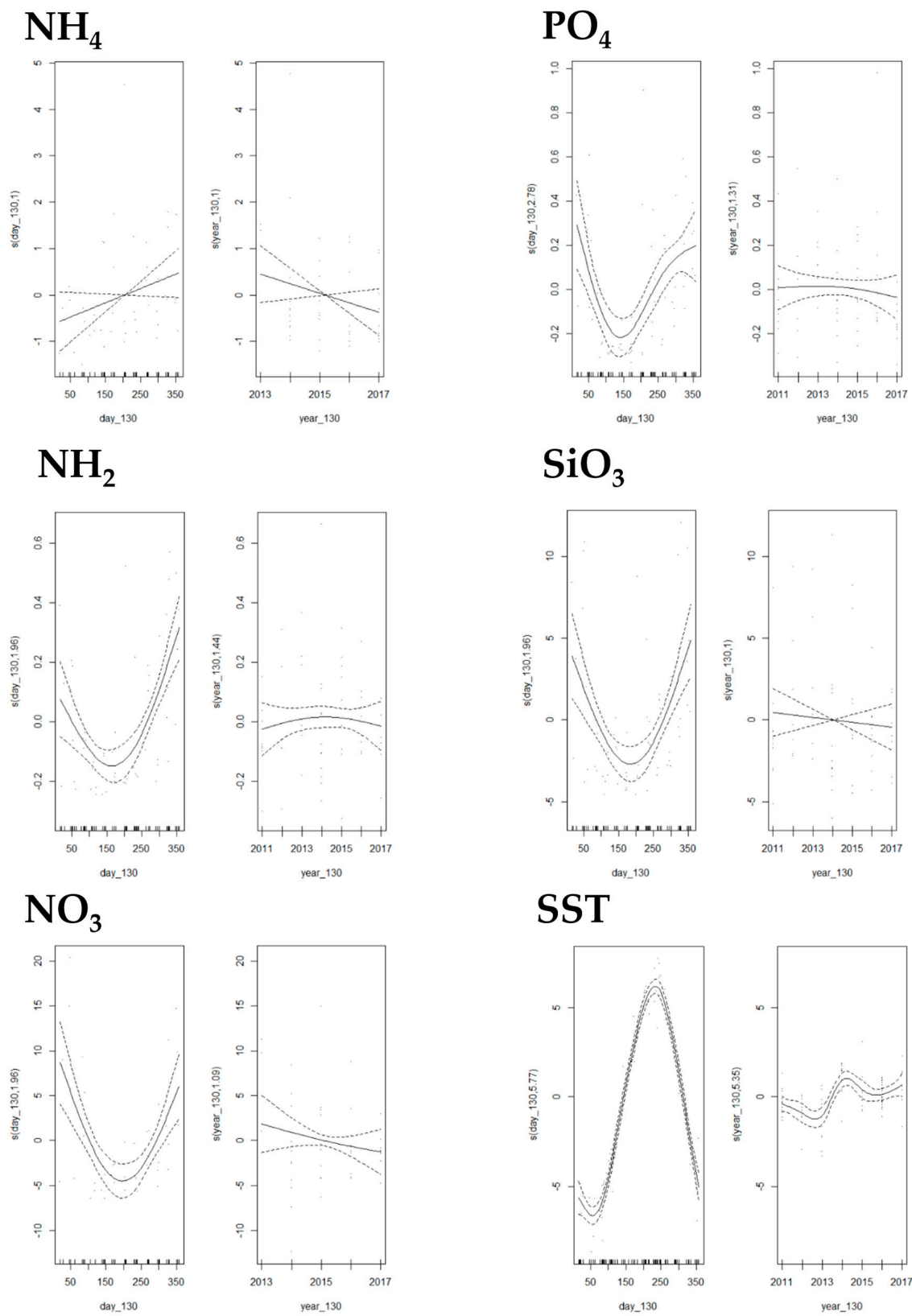


Figure A2. Smoothers for the day and year input variables, i.e., ammonium (NH_4), phosphate (PO_4), nitrite (NO_2), silicate (SiO_3), nitrate (NO_3), and the sea surface temperature (SST), for the generalised additive models in the midshore region. The smoothers are calculated from 2011 to 2017 as the three first years are used as dummy years. The solid line represents the mean value, and the dashed lines are the 95% confidence interval.

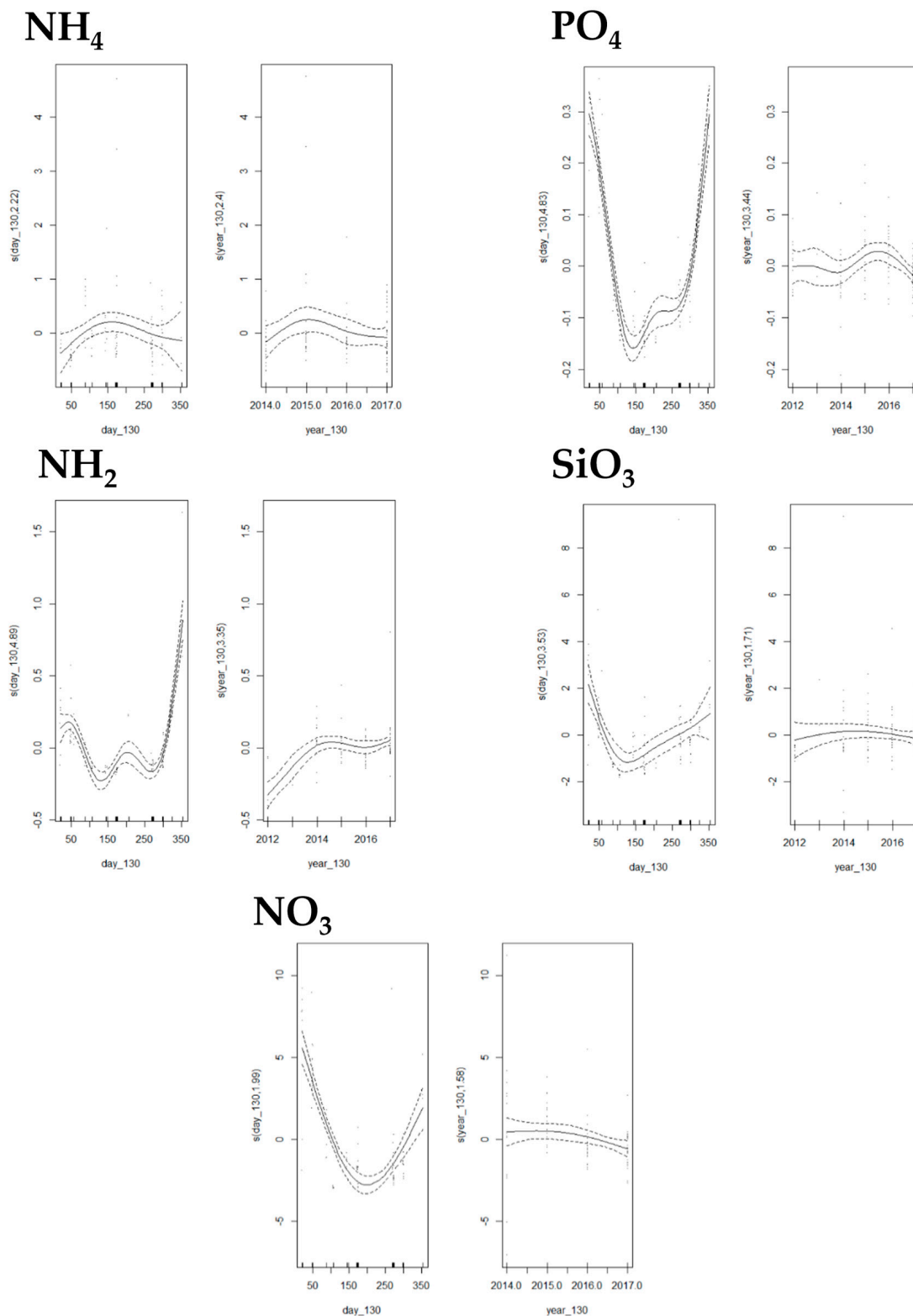


Figure A3. Smoothers for the day and year input variables, i.e., ammonium (NH_4), phosphate (PO_4), nitrite (NO_2), silicate (SiO_3), and nitrate (NO_3), for the generalised additive models (GAM) in the offshore region. The smoothers are calculated from 2011 to 2017 as the three first years are used as dummy years. The daily sea surface temperature (SST) data were extracted from the Flemish Banks Monitoring Network, and no GAMs were applied. The solid line represents the mean value, and the dashed lines are the 95% confidence interval.

Appendix D. Time Trends of the GAMs in the Three Regions of Interest

The time trends of the nutrient and SST data were created using the GAMs for each region of interest (Appendix C). The detailed comparisons of the observations are found in Tables A6 and A7 and in Figure A4. The GAMs use nonparametric smooth functions of the explanatory variables:

$$g^{-1}[E(Y_i | X_{ij})] = \alpha + \sum_{j=1}^k f_j(X_{ij}) \tag{A1}$$

where g is the link function between the expected value of nutrient concentration (Y_i) and the explanatory variables X_{ij} , with $I = 1$ to the n number of the observations and $j = 1$ to n the number explanatory variables (two explanatory variable here, i.e., time in days and years). The smoother function $f_j(X_{ij})$ quantifies the effect of the j th explanatory variable on Y_i , and α represents the estimated regression coefficient. The number of basis functions of f_j (k) represents the amount of smoothing that has been applied to the data [124]. The Rpackage “mgcv” was used to construct the GAMs [125].

Table A6. Performance of the generalised additive models in creating the daily time series of the nutrient data, i.e., dissolved inorganic nitrogen (DIN), phosphate (PO₄), silicate (SiO₃), and the sea surface temperature (SST) data in the three regions of interest. The root mean square error (RMSE) and the coefficient of determination (R²) were calculated for each nutrient and the SST against field observations per region.

Region of Interest	Nutrient and SST	RMSE	R ²
Nearshore region	DIN (mmol N m ⁻³)	9.61	0.30
	PO ₄ (mmol P m ⁻³)	0.30	0.32
	SiO ₃ (mmol Si m ⁻³)	6.43	0.39
	SST (°C)	1.82	0.94
Midshore region	DIN (mmol N m ⁻³)	5.69	0.37
	PO ₄ (mmol P m ⁻³)	0.23	0.30
	SiO ₃ (mmol Si m ⁻³)	3.65	0.29
	SST (°C)	0.88	0.96
Offshore region	DIN (mmol N m ⁻³)	2.33	0.55
	PO ₄ (mmol P m ⁻³)	0.05	0.87
	SiO ₃ (mmol Si m ⁻³)	1.30	0.30

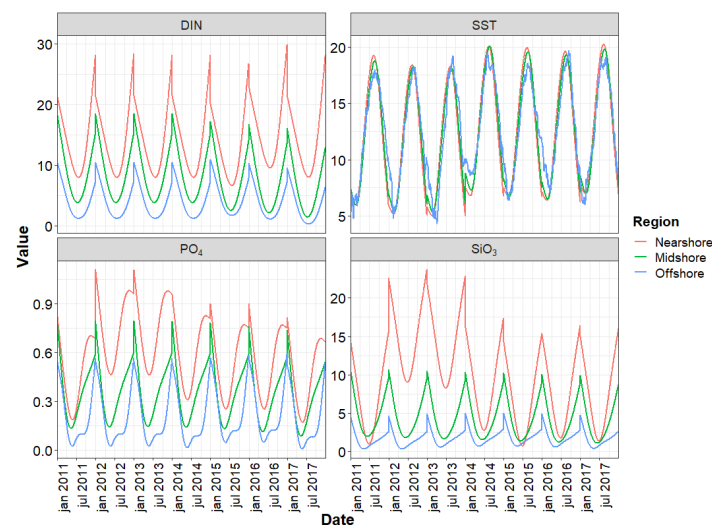


Figure A4. Time trends created using generalised additive models to generate input data for the nutrient–phytoplankton–zooplankton model. The first three years (2011 to 2013) are used as dummy years to stabilise the initial conditions of the model. These years are then removed, and the final results are only considered from 2014 to 2017.

Table A7. Performance of the different generalised additive models for each variable of interest, i.e., phosphate (PO₄), ammonium (NH₄), nitrite (NO₂), nitrate (NO₃), silicate (SiO₃), and the sea surface temperature (SST), in the nearshore, midshore, and offshore regions using data from 2011 to 2017. The number of basis functions (k) to use for each smooth term (s(day), s(year)) are included. The Akaike information criterion (AIC) and the penalised R² for adding variables to the model (adjusted R²), i.e., a p-value whether the function s() (smooth term) is non-zero, performs well (p < 0.05). The model formulation (the GAMs) is also provided. Models in bold were selected for modelling the corresponding variable.

Nearshore Region						
Variable	k-s (day)	k-s (year)	AIC	Adjusted R ²	k Performance	GAM
PO ₄	3	3	58.1	0.19	p-value < 0.05 for day, and 0.38 for year	PO ₄ ~s(day, k = ks(day)) + s(year, k = ks(year))
	4	4	50.26	0.30	p-value < 0.05 for day, and 0.23 for year	
	5	5	46.96	0.35	p-value < 0.05 for day, and 0.07 for year	
	6	6	47.6	0.36	p-value < 0.05 for day, and 0.06 for year	
NH ₄	3	3	203.54	0.04	p-values > 0.05 for both smoothers	NH ₄ ~s(day, k = ks(day)) + s(year, k = ks(year))
	4	4	201.27	0.12	p-values > 0.05 for both smoothers	
	5	5	202.06	0.11	p-values > 0.05 for both smoothers	
NO ₂	3	3	44.04	0.08	p-value < 0.05 for day, and 0.86 for year	NO ₂ ~s(day, k = ks(day)) + s(year, k = ks(year))
	4	4	33.44	0.25	p-value < 0.05 for day, and 0.79 for year	
	5	5	34.31	0.25	p-value < 0.05 for day, and 0.81 for year	
NO ₃	3	3	336.38	0.25	p-values < 0.05 for day, and 0.56 for year	NO ₃ ~s(day, k = ks(day)) + s(year, k = ks(year))
	4	4	334.55	0.31	p-values < 0.05 for day and 0.26 for year	
	5	5	335.36	0.32	p-values < 0.05 for day, and 0.24 for year.	
SiO ₃	3	3	481.08	0.28	p-value < 0.05 for day, and 0.22 for year	SiO ₃ ~s(day, k = ks(day)) + s(year, k = ks(year))
	4	4	476.2	0.35	p-value < 0.05 for both smoothers	
	5	5	471.5	0.41	p-value < 0.05 for both smoothers	
	6	6	472.28	0.41	p-value < 0.05 for both smoothers	
Midshore Region						
Variable	k-s (day)	k-s (year)	AIC	Adjusted R ²	k Performance	GAM
PO ₄	3	3	10.82	0.21	p-values < 0.05 for day, and 0.67 for year	PO ₄ ~s(day, k = ks(day)) + s(year, k = ks(year))
	4	4	4.53	0.30	p-values < 0.05 for day, and 0.71 for year	
	5	5	4.96	0.31	p-values < 0.05 for day, and 0.69 for year	
NH ₄	3	3	136.188	0.09	p-values > 0.05 for both smoothers	NH ₄ ~s(day, k = ks(day)) + s(year, k = ks(year))
	4	4	136.19	0.09	p-values > 0.05 for both smoothers	
	5	5	136.188	0.09	p-values > 0.05 for both smoothers	
NO ₂	3	3	-27.8	0.37	p-values < 0.05 for day, and 0.68 for year	NO ₂ ~s(day, k = ks(day)) + s(year, k = ks(year))
	4	4	-26.36	0.37	p-values < 0.05 for day, and 0.72 for year	
	5	5	-25.81	0.37	p-values < 0.05 for day, and 0.72 for year	
NO ₃	3	3	271.38	0.37	p-values < 0.05 for day, and 0.31 for year	NO ₃ ~s(day, k = ks(day)) + s(year, k = ks(year))
	4	4	273.25	0.38	p-values < 0.05 for day, and 0.41 for year	
	5	5	274.05	0.38	p-values < 0.05 for day, and 0.39 for year	
SiO ₃	3	3	362.68	0.28	p-value < 0.05 for day, and 0.54 for year	SiO ₃ ~s(day, k = ks(day)) + s(year, k = ks(year))
	4	4	363.23	0.28	p-value < 0.05 for day, and 0.56 for year	
	5	5	363.47	0.28	p-value < 0.05 for day, and 0.55 for year	

Table A7. Cont.

Offshore Region						
Variable	k-s(day)	k-s(year)	AIC	Adjusted R ²	k Performance	GAM
PO ₄	3	3	-281.69	0.80	<i>p</i> -value < 0.05 for both smoothers	PO ₄ ~s(day, k = ks(day)) + s(year, k = ks(year))
	4	4	-288.22	0.82	<i>p</i> -values < 0.05 for both smoothers	
	5	5	-306.43	0.84	<i>p</i> -values < 0.05 for both smoothers	
	6	6	-327.19	0.87	<i>p</i> -values < 0.05 for both smoothers	
NH ₄	3	3	232.78	0.05	<i>p</i> -values ≥ 0.05 for both smoothers	NH ₄ ~s(day, k = ks(day)) + s(year, k = ks(year))
	4	4	230.73	0.09	<i>p</i> -values > 0.05 for both smoothers	
NO ₂	3	3	-46.83	0.37	<i>p</i> -values < 0.05 for both smoothers	NO ₂ ~s(day, k = ks(day)) + s(year, k = ks(year))
	4	4	-72.92	0.51	<i>p</i> -values < 0.05 for both smoothers	
	5	5	-92.81	0.60	<i>p</i> -values < 0.05 for both smoothers	
	6	6	-125.85	0.70	<i>p</i> -values < 0.05 for both smoothers	
NO ₃	3	3	430.44	0.62	<i>p</i> -values < 0.05 for day, and 0.10 for year	NO ₃ ~s(day, k = ks(day)) + s(year, k = ks(year))
	4	4	431.57	0.62	<i>p</i> -values < 0.05 for day, and 0.14 for year	
SiO ₃	3	3	401.81	0.26	<i>p</i> -values < 0.05 for day, and 0.07 for year	SiO ₃ ~s(day, k = ks(day)) + s(year, k = ks(year))
	4	4	399.83	0.28	<i>p</i> -value < 0.05 for day, and 0.37 for year	
	5	5	396.58	0.31	<i>p</i> -value < 0.05 for day, and 0.47 for year	
	6	6	396.99	0.31	<i>p</i> -value < 0.05 for day, and 0.47 for year	

Appendix E. Model Validation: Observation versus Simulation

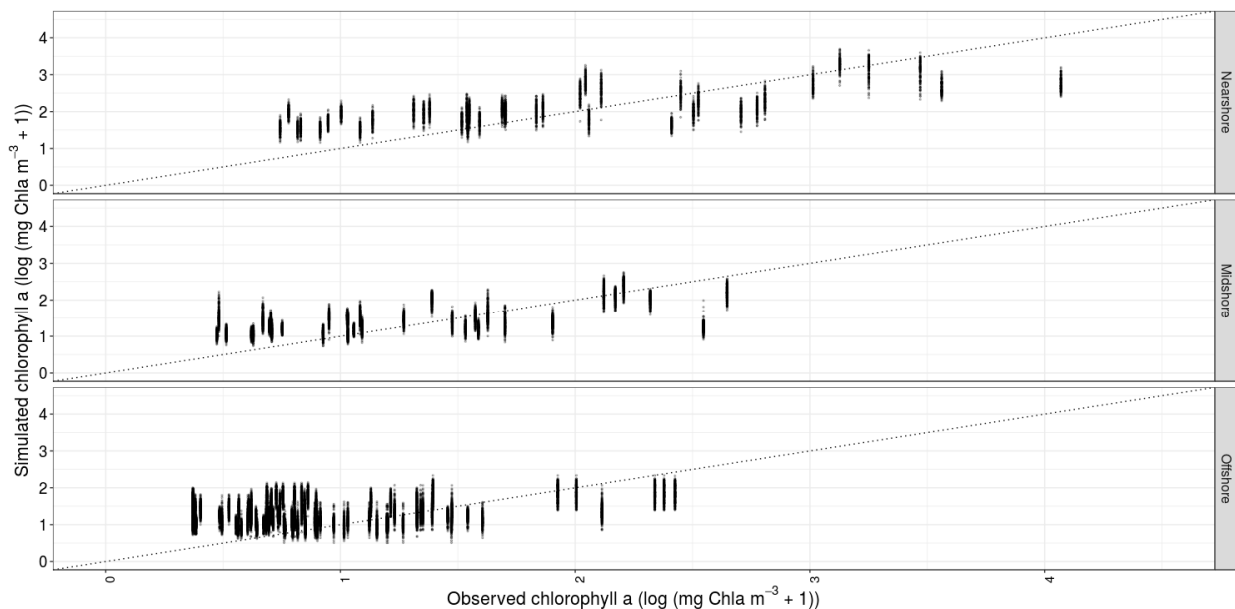


Figure A5. Phytoplankton density simulations versus the observations for the nearshore, midshore, and offshore regions in the Belgian part of the North Sea. The simulated phytoplankton densities were obtained from the best 10% simulations used to calculate the relative contributions. The dotted line represents the points' locations if all simulated values matched the observations.

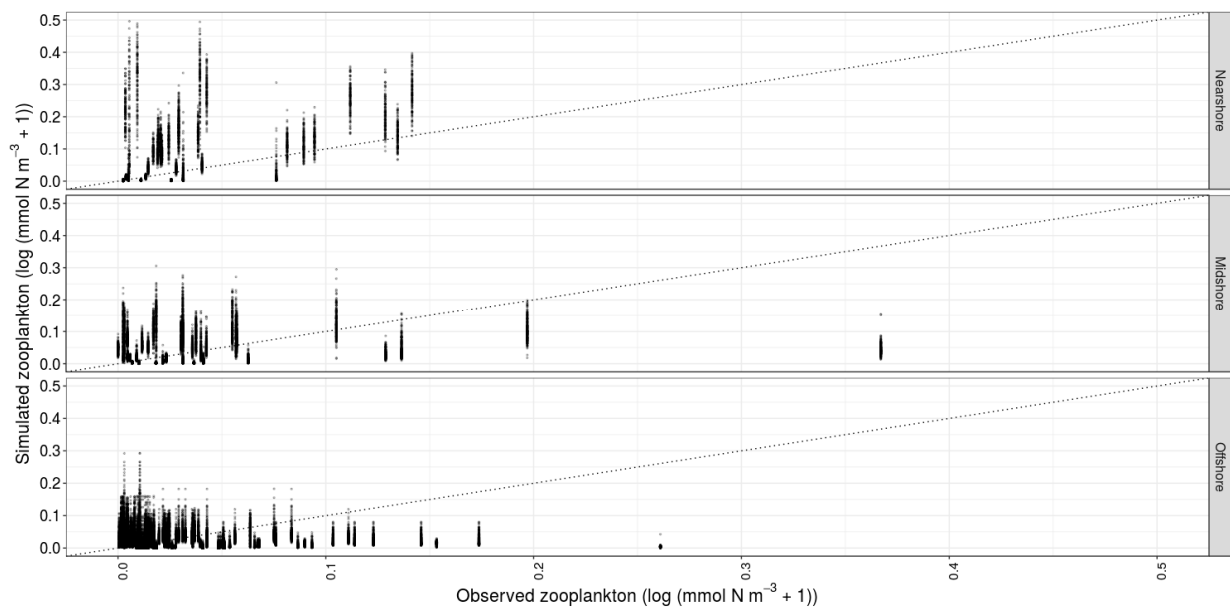


Figure A6. Zooplankton density simulations versus observations for the nearshore, midshore, and offshore regions in the Belgian part of the North Sea. The simulated zooplankton densities were obtained from the best 10% simulations used to calculate the relative contributions. The dotted line represents the points' locations if all simulated values matched the observations.

Appendix F. Simulated Zooplankton Abundances

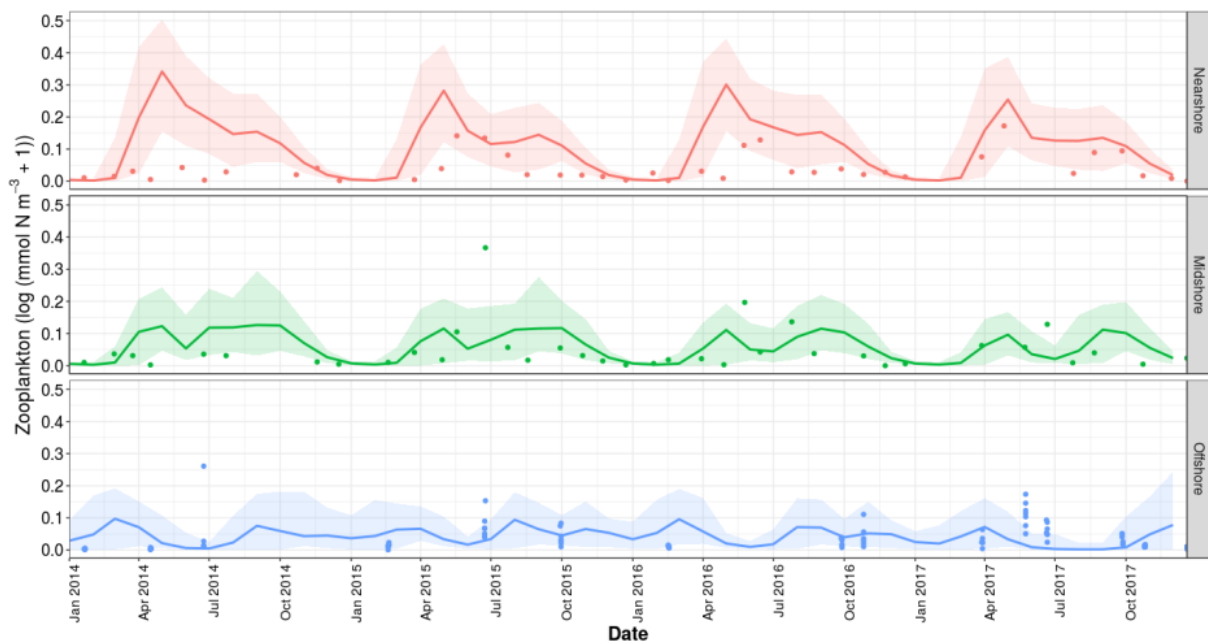


Figure A7. The zooplankton density simulations using the nutrient–phytoplankton–zooplankton model in the nearshore, midshore, and offshore regions in the Belgian part of the North Sea. The bold lines indicate the average zooplankton density predictions, and the shaded regions represent the 95% confidence interval. The dots are the observed values collected during the LifeWatch campaigns.

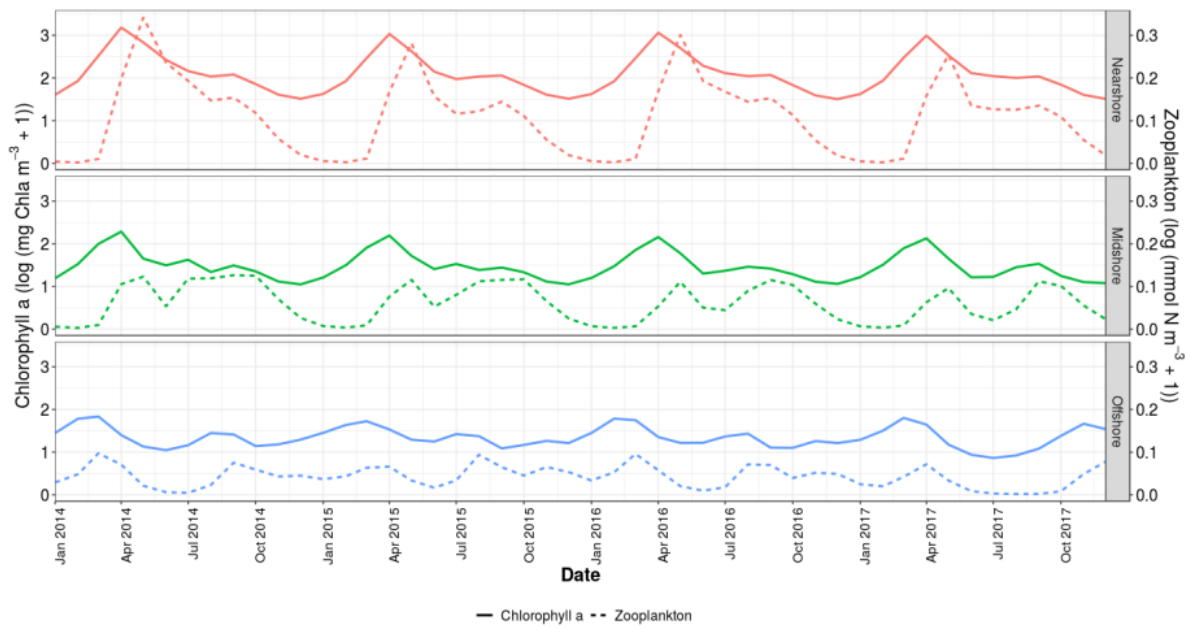


Figure A8. Phyto- and zooplankton density simulations using the nutrient–phytoplankton–zooplankton model in the nearshore, midshore, and offshore regions in the Belgian part of the North Sea. The lines represent the average phyto- and zooplankton density predictions.

Appendix G. The Relative Contributions of the Determinants of Phytoplankton Biomass Dynamics in the Near-, Mid-, and Offshore Regions

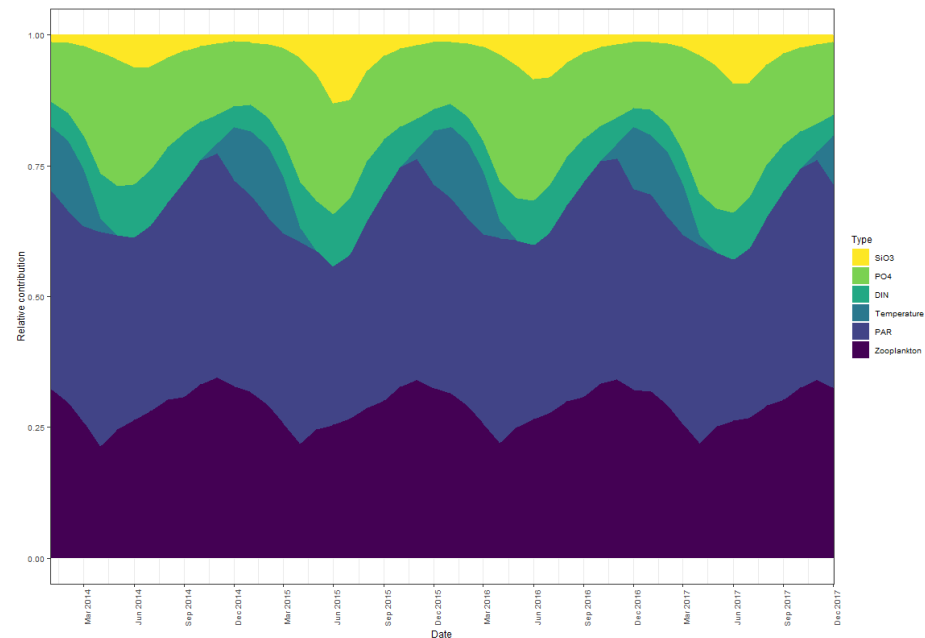


Figure A9. Average monthly relative contributions for each determinant of the phytoplankton biomass dynamics in the nearshore region. Potential determinants are dissolved inorganic nitrogen (DIN), phosphate (PO₄), silicate (SiO₃), photosynthetically active radiation (PAR), the sea surface temperature (SST), and zooplankton grazing.

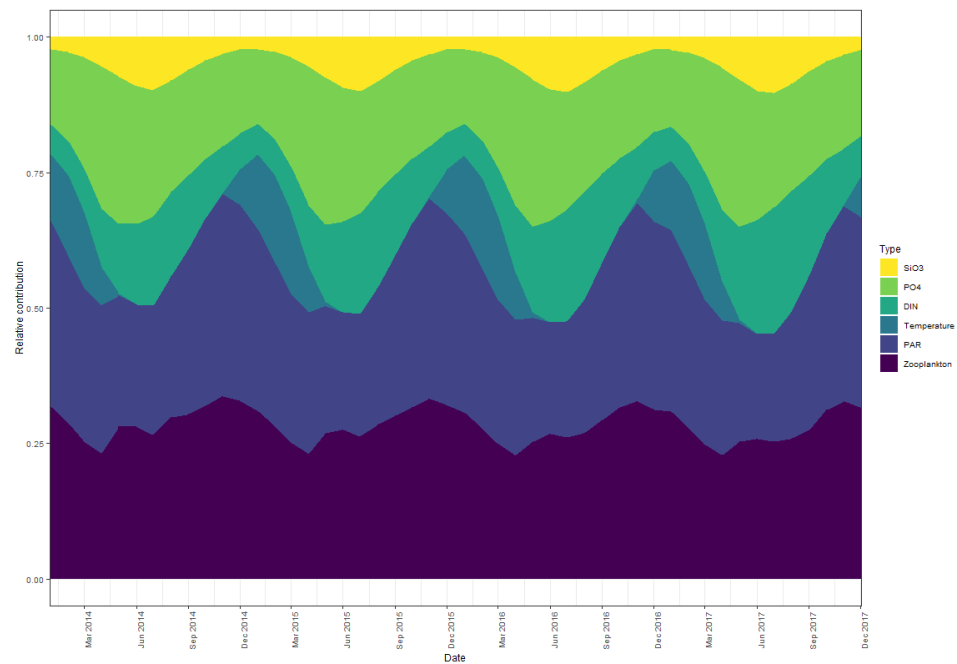


Figure A10. Average monthly relative contributions for each determinant of phytoplankton biomass dynamics in the midshore regions. Potential determinants are dissolved inorganic nitrogen (DIN), phosphate (PO₄), silicate (SiO₃), photosynthetically active radiation (PAR), the sea surface temperature (SST), and zooplankton grazing.

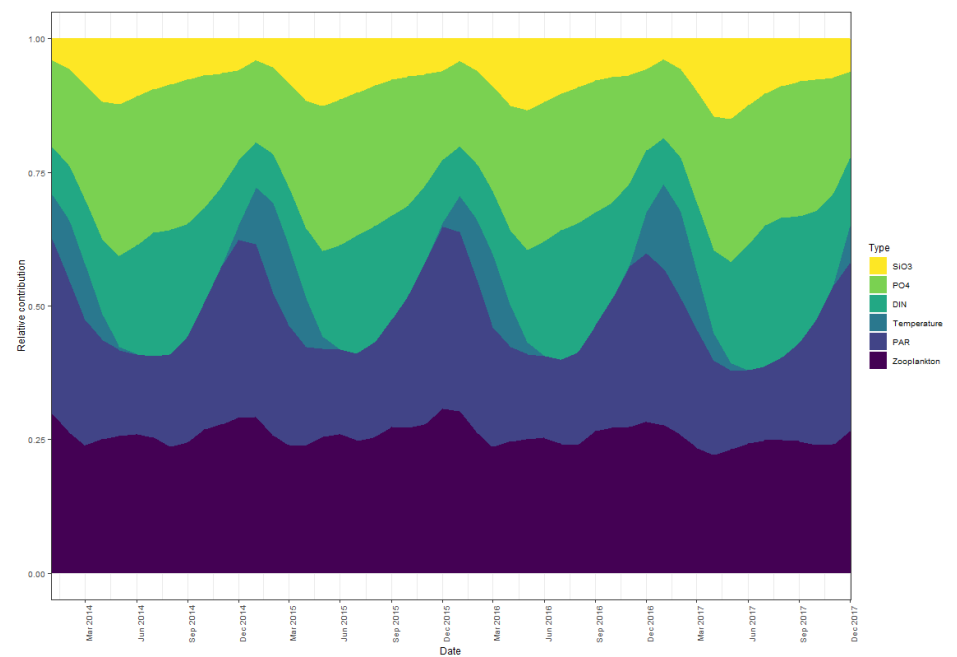


Figure A11. Average monthly relative contributions for each determinant of the phytoplankton biomass dynamics in the offshore region. Potential determinants are dissolved inorganic nitrogen (DIN), phosphate (PO₄), silicate (SiO₃), photosynthetically active radiation (PAR), the sea surface temperature (SST), and zooplankton grazing.

Appendix H. Diatom Cell Density in 2017

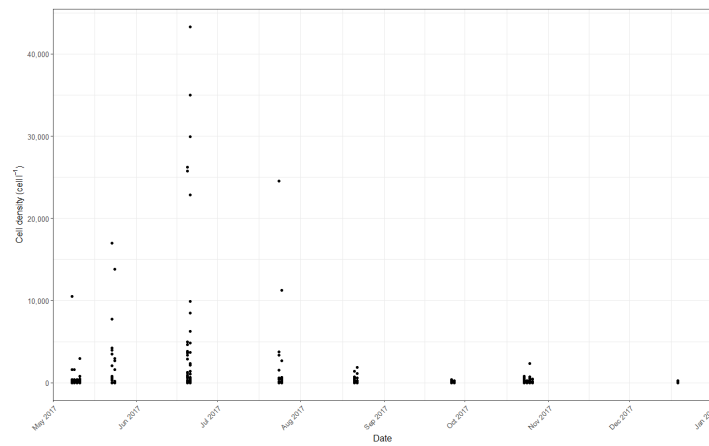


Figure A12. Diatom cell density in 2017 observed with the LifeWatch Flowcam.

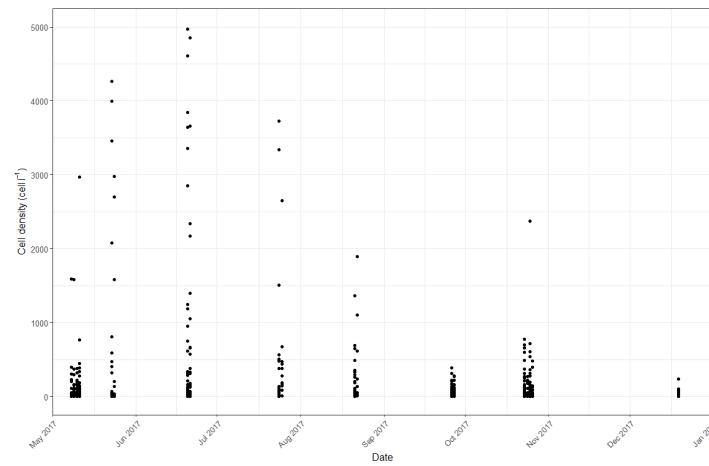


Figure A13. Diatom cell density in 2017 observed with the LifeWatch Flowcam with a y -axis limited at 5000 cell L^{-1} .

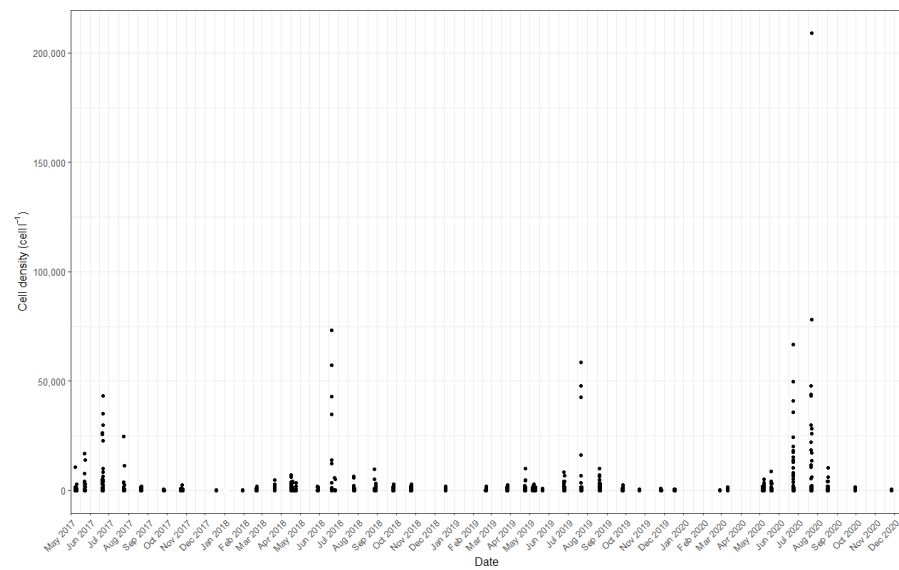


Figure A14. Diatom cell density from May 2017 to December 2020 observed with the LifeWatch Flowcam.

References

- Field, C.B.; Behrenfeld, M.J.; Randerson, J.T.; Falkowski, P. Primary Production of the Biosphere. *Science* **1998**, *281*, 237–240. [[CrossRef](#)] [[PubMed](#)]
- Carr, M.E.; Friedrichs, M.A.M.; Schmeltz, M.; Noguchi Aita, M.; Antoine, D.; Arrigo, K.R.; Asanuma, I.; Aumont, O.; Barber, R.; Behrenfeld, M.; et al. A Comparison of Global Estimates of Marine Primary Production from Ocean Color. *Deep. Sea Res. 2 Top. Stud. Oceanogr.* **2006**, *53*, 741–770. [[CrossRef](#)]
- de Baar, H. Von Liebig's Law of the Minimum and Plankton Ecology. *Prog. Oceanogr.* **1994**, *33*, 347–386. [[CrossRef](#)]
- Harpole, W.S.; Ngai, J.T.; Cleland, E.E.; Seabloom, E.W.; Borer, E.T.; Bracken, M.E.S.; Elser, J.J.; Gruner, D.S.; Hillebrand, H.; Shurin, J.B.; et al. Nutrient Co-Limitation of Primary Producer Communities. *Ecol. Lett.* **2011**, *14*, 852–862. [[CrossRef](#)] [[PubMed](#)]
- Price, N.M.; Morel, F.M.M. Colimitation of Phytoplankton Growth by Nickel and Nitrogen. *Limnol. Oceanogr.* **1991**, *36*, 1071–1077. [[CrossRef](#)]
- Irigoiien, X.; Flynn, K.J.; Harris, R.P. Phytoplankton Blooms: A “loophole” in Microzooplankton Grazing Impact? *J. Plankton Res.* **2005**, *27*, 313–321. [[CrossRef](#)]
- Belpaeme, K.; Konings, P.; Vanhooren, S. *De Kustatlas Vlaanderen/België; Coördinatiepunt Duurzaam Kustbeheer: Oostende, Belgium*, 2011.
- Arndt, S.; Lacroix, G.; Gypens, N.; Regnier, P.; Lancelot, C. Nutrient Dynamics and Phytoplankton Development along an Estuary-Coastal Zone Continuum: A Model Study. *J. Mar. Syst.* **2011**, *84*, 49–66. [[CrossRef](#)]
- Desmit, X.; Nohe, A.; Borges, A.V.; Prins, T.; De Cauwer, K.; Lagring, R.; Van der Zande, D.; Sabbe, K. Changes in Chlorophyll Concentration and Phenology in the North Sea in Relation to De-Eutrophication and Sea Surface Warming. *Limnol. Oceanogr.* **2020**, *65*, 828–847. [[CrossRef](#)]
- Capuzzo, E.; Lynam, C.P.; Barry, J.; Stephens, D.; Forster, R.M.; Greenwood, N.; McQuatters-Gollop, A.; Silva, T.; van Leeuwen, S.M.; Engelhard, G.H. A Decline in Primary Production in the North Sea over 25 Years, Associated with Reductions in Zooplankton Abundance and Fish Stock Recruitment. *Glob. Chang. Biol.* **2018**, *24*, e352–e364. [[CrossRef](#)]
- Blauw, A.N.; Benincà, E.; Laane, R.W.P.M.; Greenwood, N.; Huisman, J. Predictability and Environmental Drivers of Chlorophyll Fluctuations Vary across Different Time Scales and Regions of the North Sea. *Prog. Oceanogr.* **2018**, *161*, 1–18. [[CrossRef](#)]
- Everaert, G.; De Laender, F.; Goethals, P.L.M.; Janssen, C.R. Relative Contribution of Persistent Organic Pollutants to Marine Phytoplankton Biomass Dynamics in the North Sea and the Kattegat. *Chemosphere* **2015**, *134*, 76–83. [[CrossRef](#)] [[PubMed](#)]
- Llope, M.; Chan, K.S.; Ciannelli, L.; Reid, P.C.; Stige, L.C.; Stenseth, N.C. Effects of Environmental Conditions on the Seasonal Distribution of Phytoplankton Biomass in the North Sea. *Limnol. Oceanogr.* **2009**, *54*, 512–524. [[CrossRef](#)]
- McQuatters-Gollop, A.; Raitsos, D.E.; Edwards, M.; Pradhan, Y.; Mee, L.D.; Lavender, S.J.; Attrill, M.J. A Long-Term Chlorophyll Data Set Reveals Regime Shift in North Sea Phytoplankton Biomass Unconnected to Nutrient Trends. *Limnol. Oceanogr.* **2007**, *52*, 635–648. [[CrossRef](#)]
- Van Lancker, V.; Baeye, M.; Evangelinos, D.; Eynde, D. *Monitoring of the Impact of the Extraction of Marine Aggregates, in Casu Sand, in the Zone of the Hinder Banks; RBINS-OD Nature: Brussels, Belgium*, 2015.
- Lacroix, G.; Ruddick, K.; Ozer, J.; Lancelot, C. Modelling the Impact of the Scheldt and Rhine/Meuse Plumes on the Salinity Distribution in Belgian Waters (Southern North Sea). *J. Sea Res.* **2004**, *52*, 149–163. [[CrossRef](#)]
- Turrell, W.R. New Hypotheses Concerning the Circulation of the Northern North Sea and Its Relation to North Sea Fish Stock Recruitment. *ICES J. Mar. Sci.* **1992**, *49*, 107–123. [[CrossRef](#)]
- Lacroix, G.; Ruddick, K.; Gypens, N.; Lancelot, C. Modelling the Relative Impact of Rivers (Scheldt/Rhine/Seine) and Western Channel Waters on the Nutrient and Diatoms/Phaeocystis Distributions in Belgian Waters (Southern North Sea). *Cont. Shelf Res.* **2007**, *27*, 1422–1446. [[CrossRef](#)]
- Soetaert, K.; Herman, P.M.J. *A Practical Guide to Ecological Modelling*; Springer: Dordrecht, The Netherlands, 2009; ISBN 978-1-4020-8623-6.
- Ivanov, E.; Capet, A.; De Borger, E.; Degraer, S.; Delhez, E.J.M.; Soetaert, K.; Vanaverbeke, J.; Grégoire, M. Offshore Wind Farm Footprint on Organic and Mineral Particle Flux to the Bottom. *Front. Mar. Sci.* **2021**, *8*, 631799. [[CrossRef](#)]
- Maes, F.; Schrijvers, J.; Vanhulle, A. *Een Zee van Ruimte: Naar Een Ruimtelijk Structuurplan Voor Het Duurzaam Beheer van de Noordzee (GAUFRE)*; Federaal Wetenschapsbeleid: Brussel, Belgium, 2020.
- Ivanov, E.; Capet, A.; Barth, A.; Delhez, E.J.M.; Soetaert, K.; Grégoire, M. Hydrodynamic Variability in the Southern Bight of the North Sea in Response to Typical Atmospheric and Tidal Regimes. Benefit of Using a High Resolution Model. *Ocean Model.* **2020**, *154*, 101682. [[CrossRef](#)]
- Mortelmans, J.; Deneudt, K.; Cattrijsse, A.; Beauchard, O.; Daveloose, I.; Vyverman, W.; Vanaverbeke, J.; Timmermans, K.; Peene, J.; Roose, P.; et al. Nutrient, Pigment, Suspended Matter and Turbidity Measurements in the Belgian Part of the North Sea. *Sci. Data* **2019**, *6*, 22. [[CrossRef](#)]
- Mortelmans, J.; Goossens, J.; Amadei Martínez, L.; Deneudt, K.; Cattrijsse, A.; Hernandez, F. LifeWatch Observatory Data: Zooplankton Observations in the Belgian Part of the North Sea. *Geosci. Data J.* **2019**, *6*, 76–84. [[CrossRef](#)]
- Flanders Marine Institute (VLIZ). *LifeWatch Observatory Data: Nutrient, Pigment, Suspended Matter and Secchi Measurements in the Belgian Part of the North Sea*; Flanders Marine Institute (VLIZ): Ostend, Belgium, 2021. [[CrossRef](#)]
- Flanders Marine Institute (VLIZ). *LifeWatch Observatory Data: Zooplankton Observations in the Belgian Part of the North Sea*; Flanders Marine Institute (VLIZ): Ostend, Belgium, 2021. [[CrossRef](#)]

27. Van Ginderdeuren, K.; Van Hoey, G.; Vincx, M.; Hostens, K. The Mesozooplankton Community of the Belgian Shelf (North Sea). *J. Sea Res.* **2014**, *85*, 48–58. [CrossRef]
28. IVA MDK Flemish Banks Monitoring Network. Available online: <https://meetnetvlaamsebanken.be/> (accessed on 30 March 2021).
29. Zuur, A.F.; Ieno, E.N.; Walker, N.; Saveliev, A.A.; Smith, G.M. *Mixed Effects Models and Extensions in Ecology with R*; Springer: New York, NY, USA, 2009; ISBN 978-0-387-87457-9.
30. R Core Team. *R: A Language and Environment for Statistical Computing*; R Foundation for Statistical Computing: Vienna, Austria, 2018.
31. Lund-Hansen, L.C. Diffuse Attenuation Coefficients Kd(PAR) at the Estuarine North Sea-Baltic Sea Transition: Time-Series, Partitioning, Absorption, and Scattering. *Estuar. Coast. Shelf Sci.* **2004**, *61*, 251–259. [CrossRef]
32. Kirk, J.T.O. Preface to the Second Edition. In *Light and Photosynthesis in Aquatic Ecosystems*; Cambridge University Press: Cambridge, UK, 1994; pp. xv–xvi.
33. Thomann, R.V.; Mueller, J.A. *Principles of Surface Water Quality Modeling and Control*; Harper-Collins: New York, NY, USA, 1987.
34. Microsoft Corporation; Weston, S. *DoParallel: Foreach Parallel Adaptor for the “Parallel” Package 2020*; Microsoft Corporation: Redmond, WA, USA, 2020.
35. Wickham, H.; François, R.; Henry, L.; Müller, K. *dplyr: A Grammar of Data Manipulation*. 2019. R Package Version 0.8.3. Available online: <https://CRAN.R-project.org/package=dplyr> (accessed on 30 March 2021).
36. Microsoft; Weston, S. *Foreach: Provides Foreach Looping Construct*; Microsoft: Redmond, WA, USA, 2022; R package version 1.5.2; Available online: <https://CRAN.R-project.org/package=foreach> (accessed on 30 March 2021).
37. Wickham, H. *Ggplot2: Elegant Graphics for Data Analysis*; Springer: New York, NY, USA, 2016.
38. Kassambara, A. *Ggpubr: “ggplot2” Based Publication Ready Plots*. 2019. R Package Version 0.2.4. Available online: <https://CRAN.R-project.org/package=ggpubr> (accessed on 30 March 2021).
39. Grolemund, G.; Wickham, H. Dates and Times Made Easy with {lubridate}. *J. Stat. Softw.* **2011**, *40*, 1–25. [CrossRef]
40. Wickham, H. The Split-Apply-Combine Strategy for Data Analysis. *J. Stat. Softw.* **2011**, *40*, 1–29. [CrossRef]
41. Neuwirth, E. *RColorBrewer: ColorBrewer Palettes*. 2014. R Package Version 1.1-2. Available online: <https://CRAN.R-project.org/package=RColorBrewer> (accessed on 30 March 2021).
42. Wickham, H. Reshaping Data with the {reshape} Package. *J. Stat. Softw.* **2007**, *21*, 1–20. [CrossRef]
43. Garnier, S. *Viridis: Default Color Maps from “Matplotlib”*. 2018. R Package Version 0.5.0. Available online: <https://github.com/sjmgarnier/viridis> (accessed on 30 March 2021).
44. Ryan, J.A.; Ulrich, J.M. *Xts: EXTensible Time Series*. 2020. R Package Version 0.12.1. Available online: <https://CRAN.R-project.org/package=xts> (accessed on 30 March 2021).
45. Devlin, M.J.; Barry, J.; Mills, D.K.; Gowen, R.J.; Foden, J.; Sivyer, D.; Greenwood, N.; Pearce, D.; Tett, P. Estimating the Diffuse Attenuation Coefficient from Optically Active Constituents in UK Marine Waters. *Estuar. Coast. Shelf Sci.* **2009**, *82*, 73–83. [CrossRef]
46. Gastwirth, J.L.; Gel, Y.R.; Hui, W.L.W.; Lyubchich, V.; Miao, W.; Noguchi, K. *Lawstat: Tools for Biostatistics, Public Policy, and Law*. 2020. R Package Version 3. Available online: <https://CRAN.R-project.org/package=lawstat> (accessed on 30 March 2021).
47. Dinno, A. *Dunn.Test: Dunn’s Test of Multiple Comparisons Using Rank Sums*. 2017. R Package Version 1.3.5. Available online: <https://CRAN.R-project.org/package=dunn.test> (accessed on 30 March 2021).
48. Muylaert, K.; Gonzales, R.; Franck, M.; Lionard, M.; Van der Zee, C.; Cattrijsse, A.; Sabbe, K.; Chou, L.; Vyverman, W. Spatial Variation in Phytoplankton Dynamics in the Belgian Coastal Zone of the North Sea Studied by Microscopy, HPLC-CHEMTAX and Underway Fluorescence Recordings. *J. Sea Res.* **2006**, *55*, 253–265. [CrossRef]
49. Lancelot, C.; Spitz, Y.; Gypens, N.; Ruddick, K.; Becquevort, S.; Rousseau, V.; Lacroix, G.; Billen, G. Modelling Diatom and Phaeocystis Blooms and Nutrient Cycles in the Southern Bight of the North Sea: The MIRO Model. *Mar. Ecol. Prog. Ser.* **2005**, *289*, 63–78. [CrossRef]
50. Alvarez-Fernandez, S.; Riegman, R. Chlorophyll in North Sea Coastal and Offshore Waters Does Not Reflect Long Term Trends of Phytoplankton Biomass. *J. Sea Res.* **2014**, *91*, 35–44. [CrossRef]
51. European Environment Agency (EEA). *Mean Chlorophyll-a (Chla) Concentrations in European Seas, 2013–2017*; European Environment Agency (EEA): Copenhagen, Denmark, 2019.
52. Colella, S.; Falcini, F.; Rinaldi, E.; Sammartino, M.; Santoleri, R. Mediterranean Ocean Colour Chlorophyll Trends. *PLoS ONE* **2016**, *11*, e0155756. [CrossRef]
53. Lundsør, E.; Stige, L.C.; Sørensen, K.; Edvardsen, B. Long-Term Coastal Monitoring Data Show Nutrient-Driven Reduction in Chlorophyll. *J. Sea Res.* **2020**, *164*, 101925. [CrossRef]
54. Xu, X.; Lemmen, C.; Wirtz, K.W. Less Nutrients but More Phytoplankton: Long-Term Ecosystem Dynamics of the Southern North Sea. *Front. Mar. Sci.* **2020**, *7*, 662. [CrossRef]
55. Jiang, L.; Gerkema, T.; Kromkamp, J.C.; Van Der Wal, D.; Manuel Carrasco De La Cruz, P.; Soetaert, K. Drivers of the Spatial Phytoplankton Gradient in Estuarine-Coastal Systems: Generic Implications of a Case Study in a Dutch Tidal Bay. *Biogeosciences* **2020**, *17*, 4135–4152. [CrossRef]

56. Nohe, A.; Goffin, A.; Tyberghein, L.; Lagring, R.; De Cauwer, K.; Vyverman, W.; Sabbe, K. Marked Changes in Diatom and Dinoflagellate Biomass, Composition and Seasonality in the Belgian Part of the North Sea between the 1970s and 2000s. *Sci. Total Environ.* **2020**, *716*, 136316. [[CrossRef](#)]
57. Speeckaert, G.; Borges, A.V.; Champenois, W.; Royer, C.; Gypens, N. Annual Cycle of Dimethylsulfoniopropionate (DMSP) and Dimethylsulfoxide (DMSO) Related to Phytoplankton Succession in the Southern North Sea. *Sci. Total Environ.* **2018**, *622–623*, 362–372. [[CrossRef](#)]
58. Flanders Marine Institute (VLIZ). *LifeWatch Observatory Data: Phytoplankton Observations by Imaging Flow Cytometry (FlowCam) in the Belgian Part of the North Sea*; Flanders Marine Institute (VLIZ): Ostend, Belgium, 2021. [[CrossRef](#)]
59. Martínez, L.A.; Mortelmans, J.; Dillen, N.; Debusschere, E.; Deneudt, K. LifeWatch Observatory Data: Phytoplankton Observations in the Belgian Part of the North Sea. *Biodivers. Data J.* **2020**, *8*, e57236. [[CrossRef](#)] [[PubMed](#)]
60. Deschutter, Y.; Everaert, G.; De Schamphelaere, K.; De Troch, M. Relative Contribution of Multiple Stressors on Copepod Density and Diversity Dynamics in the Belgian Part of the North Sea. *Mar. Pollut. Bull.* **2017**, *125*, 350–359. [[CrossRef](#)]
61. Brylinski, J.M. The Pelagic Copepods in the Strait of Dover (Eastern English Channel). A Commented Inventory 120 Years after Eugène Canu. *Cah. Biol. Mar.* **2009**, *50*, 251–260.
62. Wright, J.C. The Limnology of Canyon Ferry Reservoir. I. Phytoplankton-Zooplankton Relationships in the Euphotic Zone During September and October, 1956. *Limnol. Oceanogr.* **1958**, *3*, 150–159. [[CrossRef](#)]
63. Behrenfeld, M.J.; Boss, E.S. Student's Tutorial on Bloom Hypotheses in the Context of Phytoplankton Annual Cycles. *Glob. Chang. Biol.* **2018**, *24*, 55–77. [[CrossRef](#)]
64. Mortelmans, J.; Aubert, A.; Reubens, J.; Otero, V.; Deneudt, K.; Mees, J. Copepods (Crustacea: Copepoda) in the Belgian Part of the North Sea: Trends, Dynamics and Anomalies. *J. Mar. Syst.* **2021**, *220*, 103558. [[CrossRef](#)]
65. Leitão, S.N.; Junior, M.D.M.; Porto Neto, F.D.F.; Silva, A.P.; Garcia Diaz, X.F.; e Silva, T.D.A.; Vieira, D.A.D.N.; Figueiredo, L.G.P.; da Costa, A.E.S.F.; de Santana, J.R.; et al. Connectivity between Coastal and Oceanic Zooplankton from Rio Grande Do Norte in the Tropical Western Atlantic. *Front. Mar. Sci.* **2019**, *6*, 287. [[CrossRef](#)]
66. Moore, E.; Sander, F. A Comparative Study of Zooplankton from Oceanic, Shelf, and Harbor Waters of Jamaica. *Assoc. Trop. Biol. Conserv.* **1979**, *11*, 196–206. [[CrossRef](#)]
67. Reece, J.B.; Urry, L.A.; Cain, M.L.; Wasserman, S.A.; Minorsky, P.V.; Jackson, R.B. Photosynthesis. In *Campbell Biology*, 9th ed.; Benjamin Cummings: San Francisco, CA, USA, 2011; pp. 230–251.
68. Trombetta, T.; Vidussi, F.; Mas, S.; Parin, D.; Simier, M.; Mostajir, B. Water Temperature Drives Phytoplankton Blooms in Coastal Waters. *PLoS ONE* **2019**, *14*, e0214933. [[CrossRef](#)]
69. Edwards, K.F.; Thomas, M.K.; Klausmeier, C.A.; Litchman, E. Phytoplankton Growth and the Interaction of Light and Temperature: A Synthesis at the Species and Community Level. *Limnol. Oceanogr.* **2016**, *61*, 1232–1244. [[CrossRef](#)]
70. van der Zee, C.; Chou, L. Seasonal Cycling of Phosphorus in the Southern Bight of the North Sea. *Biogeosciences* **2005**, *2*, 27–42. [[CrossRef](#)]
71. Gowen, R.J.; McCullough, G.; Kleppel, G.S.; Houchin, L.; Elliott, P. Are Copepods Important Grazers of the Spring Phytoplankton Bloom in the Western Irish Sea? *J. Plankton Res.* **1999**, *21*, 465–483. [[CrossRef](#)]
72. Burson, A.; Stomp, M.; Akil, L.; Brussaard, C.P.D.; Huisman, J. Unbalanced Reduction of Nutrient Loads Has Created an Offshore Gradient from Phosphorus to Nitrogen Limitation in the North Sea. *Limnol. Oceanogr.* **2016**, *61*, 869–888. [[CrossRef](#)]
73. Fettweis, M.; Van Den Eynde, D. The Mud Deposits and the High Turbidity in the Belgian-Dutch Coastal Zone, Southern Bight of the North Sea. *Cont. Shelf Res.* **2003**, *23*, 669–691. [[CrossRef](#)]
74. Ruddick, K.; Lacroix, G. Hydrodynamics and Meteorology of the Belgian Coastal Zone. In *Current Status of Eutrophication in the Belgian Coastal Zone*; Rousseau, V., Lancelot, C., Cox, D., Eds.; Presses Universitaires de Bruxelles: Bruxelles, Belgium, 2006.
75. Belgische Staat Initiële Beoordeling Voor de Belgische Mariene Wateren. *Kaderrichtlijn Mariene Strategie—Art 8 Lid 1a & 1b*; Belgische Staat Initiële Beoordeling Voor de Belgische Mariene Wateren: Brussels, Belgium, 2012.
76. Rousseau, V.; Youngje, P.; Ruddick, K.; Vyverman, W.; Parent, J.Y.; Lancelot, C. Phytoplankton Blooms in Response to Nutrient Enrichment. In *Current Status of Eutrophication in the Belgian Coastal Zone*; Rousseau, V., Lancelot, C., Cox, D., Eds.; Presses Universitaires de Bruxelles: Bruxelles, Belgium, 2006.
77. van Leeuwen, S.; Tett, P.; Mills, D.; van der Molen, J. Stratified and Nonstratified Areas in the North Sea: Long-term Variability and Biological and Policy Implications. *J. Geophys. Res. Oceans* **2015**, *120*, 4670–4686. [[CrossRef](#)]
78. Richard, M.; Archambault, P.; Thouzeau, G.; Desrosiers, G. Influence of Suspended Mussel Lines on the Biogeochemical Fluxes in Adjacent Water in the Îles-de-La-Madeleine (Quebec, Canada). *Can. J. Fish. Aquat. Sci.* **2006**, *63*, 1198–1213. [[CrossRef](#)]
79. Nizzoli, D.; Welsh, D.T.; Viaroli, P. Seasonal Nitrogen and Phosphorus Dynamics during Benthic Clam and Suspended Mussel Cultivation. *Mar. Pollut. Bull.* **2011**, *62*, 1276–1287. [[CrossRef](#)]
80. Cugier, P.; Struski, C.; Blanchard, M.; Mazurié, J.; Pouvreau, S.; Olivier, F.; Trigui, J.R.; Thiébaud, E. Assessing the Role of Benthic Filter Feeders on Phytoplankton Production in a Shellfish Farming Site: Mont Saint Michel Bay, France. *J. Mar. Syst.* **2010**, *82*, 21–34. [[CrossRef](#)]
81. Nielsen, T.G.; Maar, M. Effects of a Blue Mussel *Mytilus Edulis* Bed on Vertical Distribution and Composition of the Pelagic Food Web. *Mar. Ecol. Prog. Ser.* **2007**, *339*, 185–198. [[CrossRef](#)]
82. Forster, R. *The Effect of Monopile-Induced Turbulence on Local Suspended Sediment Pattern around UK Wind Farms: Field Survey*; The Crown Estate: London, UK, 2018.

83. Flynn, K.J.; Mitra, A.; Wilson, W.H.; Kimmance, S.A.; Clark, D.R.; Pelusi, A.; Polimene, L. 'Boom-and-busted' Dynamics of Phytoplankton–Virus Interactions Explain the Paradox of the Plankton. *New Phytol.* **2022**, *234*, 990–1002. [[CrossRef](#)]
84. Brussaard, C.P.D. Viral Control of Phytoplankton Populations—A Review. *J. Eukaryot. Microbiol.* **2004**, *51*, 125–138. [[CrossRef](#)]
85. Biggs, T.E.G.; Huisman, J.; Brussaard, C.P.D. Viral Lysis Modifies Seasonal Phytoplankton Dynamics and Carbon Flow in the Southern Ocean. *ISME J.* **2021**, *15*, 3615–3622. [[CrossRef](#)]
86. Holmström, K.E.; Järnberg, U.; Bignert, A. Temporal Trends of PFOS and PFOA in Guillemot Eggs from the Baltic Sea, 1968–2003. *Environ. Sci. Technol.* **2005**, *39*, 80–84. [[CrossRef](#)]
87. Coull, B.C.; Chandler, G.T. Pollution and Meiofauna—Field, Laboratory, and Mesocosm Studies. *Oceanogr. Mar. Biol.* **1992**, *30*, 191–271.
88. Schlüter, M.H.; Kraberg, A.; Wiltshire, K.H. Long-Term Changes in the Seasonality of Selected Diatoms Related to Grazers and Environmental Conditions. *J. Sea Res.* **2012**, *67*, 91–97. [[CrossRef](#)]
89. Berdalet, E.; Peters, F.; Koumandou, V.L.; Roldán, C.; Guadayol, Ò.; Estrada, M. Species-Specific Physiological Response of Dinoflagellates to Quantified Small-Scale Turbulence. *J. Phycol.* **2007**, *43*, 965–977. [[CrossRef](#)]
90. Jakobsen, H.H.; Markager, S. Carbon-to-Chlorophyll Ratio for Phytoplankton in Temperate Coastal Waters: Seasonal Patterns and Relationship to Nutrients. *Limnol. Oceanogr.* **2016**, *61*, 1853–1868. [[CrossRef](#)]
91. Butenschön, M.; Clark, J.; Aldridge, J.N.; Icarus Allen, J.; Artioli, Y.; Blackford, J.; Bruggeman, J.; Cazenave, P.; Ciavatta, S.; Kay, S.; et al. ERSEM 15.06: A Generic Model for Marine Biogeochemistry and the Ecosystem Dynamics of the Lower Trophic Levels. *Geosci. Model. Dev.* **2016**, *9*, 1293–1339. [[CrossRef](#)]
92. Pätsch, J.; Kühn, W. Nitrogen and Carbon Cycling in the North Sea and Exchange with the North Atlantic—A Model Study. Part I. Nitrogen Budget and Fluxes. *Cont. Shelf Res.* **2008**, *28*, 767–787. [[CrossRef](#)]
93. Capuzzo, E.; Stephens, D.; Silva, T.; Barry, J.; Forster, R.M. Decrease in Water Clarity of the Southern and Central North Sea during the 20th Century. *Glob. Chang. Biol.* **2015**, *21*, 2206–2214. [[CrossRef](#)]
94. Zscheischler, J.; Westra, S.; van den Hurk, B.J.J.M.; Seneviratne, S.I.; Ward, P.J.; Pitman, A.; AghaKouchak, A.; Bresch, D.N.; Leonard, M.; Wahl, T.; et al. Future Climate Risk from Compound Events. *Nat. Clim. Chang.* **2018**, *8*, 469–477. [[CrossRef](#)]
95. IPCC. *IPCC Special Report on the Ocean and Cryosphere in a Changing Climate*; Pörtner, H.-O., Roberts, D.C., Alegría, A., Nicolai, M., Okem, A., Petzold, J., Rama, B., Weyer, N.M., Eds.; Cambridge University Press: Cambridge, UK, 2019.
96. Paerl, H.W.; Valdes, L.M.; Peierls, B.L.; Adolf, J.E.; Harding, L.W. Part 2: Eutrophication of Freshwater and Marine Ecosystems. *Limnol. Oceanogr.* **2006**, *51*, 351–355.
97. IPCC. Summary for Policymakers. In *Climate Change 2021: The Physical Science Basis. Contribution of Working Group I to the Sixth Assessment Report of the Intergovernmental Panel on Climate Change*; Masson-Delmotte, B.Z., Zhai, V.P., Pirani, A., Connors, S.L., Péan, C., Berger, S., Caud, N., Chen, Y., Goldfarb, L., Gomis, M.I., et al., Eds.; Cambridge University Press: Cambridge, UK; New York, NY, USA, 2021.
98. Benedetti, F.; Vogt, M.; Elizondo, U.H.; Righetti, D.; Zimmermann, N.E.; Gruber, N. Major Restructuring of Marine Plankton Assemblages under Global Warming. *Nat. Commun.* **2021**, *12*, 5226. [[CrossRef](#)]
99. Ferreira, A.; Costa, R.R.; Dotto, T.S.; Kerr, R.; Tavano, V.M.; Brito, A.C.; Brotas, V.; Secchi, E.R.; Mendes, C.R.B. Changes in Phytoplankton Communities Along the Northern Antarctic Peninsula: Causes, Impacts and Research Priorities. *Front. Mar. Sci.* **2020**, *7*, 576254. [[CrossRef](#)]
100. Hays, G.; Richardson, A.; Robinson, C. Climate Change and Marine Plankton. *Trends Ecol. Evol.* **2005**, *20*, 337–344. [[CrossRef](#)]
101. Chakraborty, K.; Kumar, N.; Girishkumar, M.S.; Gupta, G.V.M.; Ghosh, J.; Udaya Bhaskar, T.V.S.; Thangaprakash, V.P. Assessment of the Impact of Spatial Resolution on ROMS Simulated Upper-Ocean Biogeochemistry of the Arabian Sea from an Operational Perspective. *J. Oper. Oceanogr.* **2019**, *12*, 116–142. [[CrossRef](#)]
102. Latasa, M. Improving Estimations of Phytoplankton Class Abundances Using CHEMTAX. *Mar. Ecol. Prog. Ser.* **2007**, *329*, 13–21. [[CrossRef](#)]
103. Mackey, M.D.; Mackey, D.J.; Higgins, H.W.; Wright, S.W. CHEMTAX—A Program for Estimating Class Abundances from Chemical Markers: Application to HPLC Measurements of Phytoplankton. *Mar. Ecol. Prog. Ser.* **1996**, *144*, 265–283. [[CrossRef](#)]
104. Pan, H.; Li, A.; Cui, Z.; Ding, D.; Qu, K.; Zheng, Y.; Lu, L.; Jiang, T.; Jiang, T. A Comparative Study of Phytoplankton Community Structure and Biomass Determined by HPLC-CHEMTAX and Microscopic Methods during Summer and Autumn in the Central Bohai Sea, China. *Mar. Pollut. Bull.* **2020**, *155*, 111172. [[CrossRef](#)]
105. Wells, M.L.; Karlson, B.; Wulff, A.; Kudela, R.; Trick, C.; Asnaghi, V.; Berdalet, E.; Cochlan, W.; Davidson, K.; De Rijcke, M.; et al. Future HAB Science: Directions and Challenges in a Changing Climate. *Harmful Algae* **2020**, *91*, 101632. [[CrossRef](#)]
106. Wiltshire, K.H.; Malzahn, A.M.; Wirtz, K.; Greve, W.; Janisch, S.; Mangelsdorf, P.; Manly, B.F.J.; Boersma, M. Resilience of North Sea Phytoplankton Spring Bloom Dynamics: An Analysis of Long-Term Data at Helgoland Roads. *Limnol. Oceanogr.* **2008**, *53*, 1294–1302. [[CrossRef](#)]
107. Assante, M.; Candela, L.; Castelli, D.; Cirillo, R.; Coro, G.; Frosini, L.; Lelii, L.; Mangiacrapa, F.; Pagano, P.; Panichi, G.; et al. Enacting Open Science by D4Science. *Future Gener. Comput. Syst.* **2019**, *101*, 555–563. [[CrossRef](#)]
108. Kishi, M.J.; Kashiwai, M.; Ware, D.M.; Megrey, B.A.; Eslinger, D.L.; Werner, F.E.; Noguchi-Aita, M.; Azumaya, T.; Fujii, M.; Hashimoto, S.; et al. NEMURO—A Lower Trophic Level Model for the North Pacific Marine Ecosystem. *Ecol. Modell.* **2007**, *202*, 12–25. [[CrossRef](#)]

109. Fan, W.; Lv, X. Data Assimilation in a Simple Marine Ecosystem Model Based on Spatial Biological Parameterizations. *Ecol. Modell.* **2009**, *220*, 1997–2008. [[CrossRef](#)]
110. Cropp, R.; Norbury, J. Parameterising Competing Zooplankton for Survival in Plankton Functional Type Models. *Ecol. Modell.* **2010**, *221*, 1852–1864. [[CrossRef](#)]
111. Ruzicka, J.J.; Wainwright, T.C.; Peterson, W.T. A Simple Plankton Model for the Oregon Upwelling Ecosystem: Sensitivity and Validation against Time-Series Ocean Data. *Ecol. Modell.* **2011**, *222*, 1222–1235. [[CrossRef](#)]
112. Beşiktepe, Ş.T.; Lermusiaux, P.F.J.; Robinson, A.R. Coupled Physical and Biogeochemical Data-Driven Simulations of Massachusetts Bay in Late Summer: Real-Time and Postcruise Data Assimilation. *J. Mar. Syst.* **2003**, *40–41*, 171–212. [[CrossRef](#)]
113. Billen, G.; Garnier, J. The Phison River Plume: Coastal Eutrophication in Response to Changes in Land Use and Water Management in the Watershed. *Aquat. Microb. Ecol.* **1997**, *13*, 3–17. [[CrossRef](#)]
114. Brandt, G.; Wirtz, K.W. Interannual Variability of Alongshore Spring Bloom Dynamics in a Coastal Sea Caused by the Differential Influence of Hydrodynamics and Light Climate. *Biogeosciences* **2010**, *7*, 371–386. [[CrossRef](#)]
115. Xu, J.; Hood, R.R. Modeling Biogeochemical Cycles in Chesapeake Bay with a Coupled Physical-Biological Model. *Estuar. Coast. Shelf Sci.* **2006**, *69*, 19–46. [[CrossRef](#)]
116. Brun, P.; Payne, M.R.; Kiørboe, T. A Trait Database for Marine Copepods. *Earth Syst. Sci. Data* **2016**, *9*, 99–113. [[CrossRef](#)]
117. Löder, M.G.J.; Kraberg, A.C.; Aberle, N.; Peters, S.; Wiltshire, K.H. Dinoflagellates and Ciliates at Helgoland Roads, North Sea. *Helgol. Mar. Res.* **2012**, *66*, 11–23. [[CrossRef](#)]
118. Sautour, B.; Castel, J. Spring Zooplankton Distribution and Production of the Copepod *Euterpina Acutifrons* in Marennes-Oléron Bay (France). *Hydrobiologia* **1995**, *310*, 163–175. [[CrossRef](#)]
119. Lombard, F.; Renaud, F.; Sainsbury, C.; Sciandra, A.; Gorsky, G. Appendicularian Ecophysiology I: Food Concentration Dependent Clearance Rate, Assimilation Efficiency, Growth and Reproduction of *Oikopleura Dioica*. *J. Mar. Syst.* **2009**, *78*, 606–616. [[CrossRef](#)]
120. Van Nieuwerburgh, L.; Wänstrand, I.; Snoeijs, P. Growth and C:N:P Ratios in Copepods Grazing on N- or Si-Limited Phytoplankton Blooms. *Hydrobiologia* **2004**, *514*, 57–72. [[CrossRef](#)]
121. Tada, K.; Pithakpol, S.; Yano, R.; Montani, S. Carbon and Nitrogen Content of *Noctiluca Scintillans* in the Seto Inland Sea, Japan. *J. Plankton Res.* **2000**, *22*, 1203–1211. [[CrossRef](#)]
122. Szyper, J.P. Nutritional Depletion of the Aquaculture Feed Organisms *Euterpina Acutifrons*, *Artemia* Sp. and *Brachionus Plicatilis* During Starvation. *J. World Aquac. Soc.* **1989**, *20*, 162–169. [[CrossRef](#)]
123. Abdel-Moati, M.A.R.; Atta, M.M.; Khalil, A.N.; Nour-El-Din, N.M. Carbon, Nitrogen and Phosphorus Content of the Copepod *Euterpina Acutifrons* in the Coastal Waters of Alexandria, Egypt. *Bull. Nat. Inst. Ocn. Fish.* **1993**, 173–190.
124. Wood, S.N. *Generalized Additive Models: An Introduction with R*, 2nd ed.; Chapman and Hall/CRC: Boca Raton, FL, USA, 2017.
125. Wood, S.N. Fast Stable Restricted Maximum Likelihood and Marginal Likelihood Estimation of Semiparametric Generalized Linear Models. *J. R. Stat. Soc. B* **2011**, *73*, 3–36. [[CrossRef](#)]

Disclaimer/Publisher’s Note: The statements, opinions and data contained in all publications are solely those of the individual author(s) and contributor(s) and not of MDPI and/or the editor(s). MDPI and/or the editor(s) disclaim responsibility for any injury to people or property resulting from any ideas, methods, instructions or products referred to in the content.